Reviews in Mineralogy & Geochemistry
Vol. 62, pp. 85-115, 2006

Hydrogen in High Pressure Silicate and Oxide Mineral Structures

Joseph R. Smyth

Department of Geological Sciences
University of Colorado
Boulder, Colorado, 80309, U.S.A.
e-mail: smyth@colorado.edu

INTRODUCTION

Earth is the water planet. Liquid water covers more than 70% of the surface and dominates all surface processes, geological, meteorological, and biological. However the hydrosphere composes only about 0.025% of the planet's mass, so that small amounts of H incorporated into the oxygen minerals of the interior may constitute the majority of Earth's total water. The Earth is thought to be generally similar in composition to the chondrite meteorites which average about 0.10% by weight H_2O. So if the Earth were strictly chondritic in its H content, about 75% of that H as water would have either been tied up in the minerals of the interior or lost to space. Understanding how H behaves at the atomic scale in these materials will help us to understand how the Earth balances and retains its water and may help us to understand how water planets develop and how common they might be.

In addition to the surface processes, water also controls the processes of the interior. Water dramatically reduces the melting temperature of rocks controlling igneous processes. Even trace amounts of hydrogen have a major effect on some physical properties such as deformation strength and electrical conductivity (Karato 1990). The nominally anhydrous minerals of the Earth's interior are capable of incorporating many times the amount of water in the hydrosphere, and these phases would need to be saturated before stoichiometrically hydrous minerals could be stable. Hydrogen in amounts reported in olivine, wadsleyite, and ringwoodite by Kohlstedt et al. (1996) as recalibrated by Bell et al. (2003), if present in the Earth, would constitute a significant fraction of the total water budget of the planet. The amounts that can be incorporated into the nominally anhydrous minerals of the Transition Zone (410-660 km depth) may constitute the largest reservoir of water in the planet and may have controlled the chemical evolution and interior processes of the planet. Hirschmann et al. (2005) have estimated the storage capacities of the various mineral reservoirs in the mantle.

These volumes of water imply that there may be a deep water cycle in the Earth whereby some of the water in subducted slabs may be returned to the large deep interior reservoir and then be released in mid-ocean ridge basalts so that the amount of water in the Earth's oceans would represent a dynamic balance between these processes. This process would depend on the ability of the nominally anhydrous phases of the upper mantle to incorporate the water released by the breakdown of the hydrous phases on increasing pressure and temperature with subduction.

GEOCHEMISTRY OF H

Hydrogen is the most abundant element in the cosmos, and the geochemical behavior of hydrogen is unlike that of any other element. Because the proton does not behave like other cations in the crystal, it is generally inappropriate to treat H as an incompatible element

1529-6466/06/0062-0005$05.00 DOI: 10.2138/rmg.2006.62.5

or to compare its compatibility with other cations. In the highly reducing conditions of the condensing solar nebula, H was primarily atmophile, as the diatomic gas H_2, but also as methane, ammonia, and water. However, in the Earth's crust and mantle, hydrogen in its ionic state, H^+, is strongly lithophile. It substitutes readily in silicates and other oxygen minerals in both trace and stoichiometric amounts. Because H does not occupy a normal cation site in a mineral, it does not have an effective ionic radius that controls its geochemical behavior. Its compatibility is therefore not systematic as other trace cations are, but strongly dependent on temperature, pressure, and the chemical activity of possible charge-balancing cations.

The chalcophile nature of H is not well known, and its substitution in sulfide minerals in trace amounts is difficult to measure and poorly studied. H_2S is an abundant volatile in mafic to silicic volcanic systems, and there are a few OH-bearing sulfide minerals such as tochilinite $[6(Fe_{0.9}S)\cdot 5(Fe,Mg)(OH)_2)]$ (Beard 2000), but I was unable to identify a single H-bearing sulfide mineral that does not also contain oxygen. Under reducing conditions, neutral H is highly soluble in metallic liquids and forms solid metal hydrides. However, very little is known about H partitioning between silicate and metallic liquids, and the amount of H in the core is unknown as is its effect on liquid metal densities under conditions of the core. The objectives of this review are to examine the various structural substitution mechanisms whereby H enters major high pressure silicate and oxide minerals in stoichiometric amounts and then use this information to look at H substitution in nominally anhydrous minerals of the Earth's mantle.

CRYSTAL CHEMISTRY OF H

Because oxygen is the only anionic species of significant abundance in the crust and mantle, we think of hydrogen and water as synonymous. At low pressure, water can enter silicates either as molecular water or as hydroxyl, or both. In low-density silicates such as zeolites and clays, the water molecules are located in large cavities or interlayer sites and freely flow into and out of the crystals. In other low-temperature minerals such as gypsum, the molecular water is tightly bound structurally and does not exchange. Hydrogen also enters low temperature and pressure minerals as structural hydroxyl. At higher pressures, hydrogen occurs in the solid minerals of the mantle in several forms, but generally does not exchange. It can be present as discrete, structurally bound water molecules as in lawsonite, K-cymrite, or 10 Å phase, but most often it is present as hydroxyl, OH^-. The hydroxyl can be stoichiometric, part of the nominal mineral formula, or it can be a minor constituent, where the hydrogen may substitute ionically for other cations in the structure. In nominally hydrous silicates, the hydroxyl rarely bonds directly to the Si cation. This is also true of other small, high-field-strength cations such as B, C, P, and S^{6+}. The proton position is difficult to locate by X-ray diffraction, but neutron single-crystal or powder diffraction can give proton positions with high precision. Additionally, the protonated oxygen is relatively easy to identify from X-ray data by a simple Pauling bond strength calculation.

When H enters nominally anhydrous minerals, the proton does not occupy the normal cation position, but attaches to one or more of the oxygens. The usual proton to oxygen nucleus distance (0.95 to 1.2 Å) is less than the nominal oxygen radius (1.32 to 1.4 Å). The oxygen atoms that can be protonated in a stoichiometric, fully occupied structure are those that are most underbonded. The degree of underbonding can be calculated on the basis of Pauling bond strength or a Madelung site potential calculation. Pauling bond strength at the oxygen is calculated as the sum of the bond strengths (nominal cation valence divided by coordination number) around an oxygen atom. The Madelung site potential (Smyth 1987, 1989) is the nominal valence charge divided by distance and summed to convergence. These methods may identify the oxygen most likely to be protonated if there are several non-equivalent oxygen positions in a structure, but does not identify the proton location. Libowitzky (1999) reports a correlation of O-H-O distance with O-H stretching frequency. This has been used together

with polarization vectors to deduce proton positions in nominally anhydrous structures such as wadsleyite (Kohn et al. 2002) and akimotoite (Bolfan-Casanova et al. 2002). Ross et al. (2003) propose a computational method to identify non-bonding electron-pairs on oxygens in order to locate potential docking sites for protons in high pressure silicates. Extensive protonation of an oxygen site in a nominally anhydrous mineral generally requires a charge balancing substitution or a cation vacancy. Cation vacancies normally result in a significant expansion of the vacant coordination polyhedron, however such vacant polyhedra are typically large and highly compressible (Jacobsen 2006).

Tetrahedral cation vacancies charge-balanced by protons are well documented. This is the so-called hydrogarnet substitution because the H_4O_4 tetrahedron can completely replace the silicate tetrahedron in hydrogarnets (Lager et al. 2005). The H_4O_4 tetrahedron is larger than the silicate tetrahedron with the Si-O distance in silicate garnets being 1.60 to 1.64 Å whereas the equivalent distance ($\overline{4}$-O) in hydrogarnet is over 2.0 Å. This means that pressure will inhibit this substitution mechanism so that garnets from natural high pressure (2-5 GPa) environments generally contain less than about 50 ppmw H_2O (Bell and Rossman 1992). It may be possible that this substitution mechanism may again become viable at pressures above about 7 GPa, as it has been proposed to be present in hydrous coesite above this pressure (Koch-Mueller et al. 2003).

Oxygen-oxygen edges are typically 2.6 to 2.8 Å for tetrahedral silicon, whereas edges of Mg octahedra typically are 2.8 to 3.0 Å. These distances have been used to infer proton positions from infrared spectra based on the calibration of Libowizky (1999) (e.g., Kohn et al. 2002), however the correlation curve is quite flat in this region and cation vacancy may result in local distortion of the coordination polyhedra. Octahedral cation vacancy charge-balanced by protons appears to be more common at pressures of the upper mantle. Protonated octahedral cation vacancy appears to become a very significant substitution mechanism in olivine (Smyth et al. 2006a) and wadsleyite (Smyth et al. 1997; Ross et al. 2003; Jacobsen et al. 2005). Wadsleyite (β-Mg_2SiO_4) can contain more than 3 wt% H_2O (Inoue et al. 1995; Kohlstedt et al. 1996), where the charge balance mechanism is octahedral site vacancy, principally at M3 (Smyth et al. 1997; Kohn et al. 2003).

Even trace hydration (10 to 1000 ppmw H_2O) can have very large effects of physical properties of nominally anhydrous phases such as mechanical strength (Kavner 2003), effective viscosity (Karato et al. 1986), and electrical conductivity (Karato 1990; Huang et al. 2005). Minor hydration (1000 to 10000 ppmw H_2O) can have a major effect on density, compressibility (Smyth et al. 2003; 2004), seismic velocity (Jacobsen et al. 2005; 2006), and pressure-temperature conditions of phase transitions (Wood 1995; Smyth and Frost 2002). In order to understand the crystal chemistry of H at high pressure, it is necessary to first look briefly at the nominally hydrous phases on the Earth's mantle and then to examine the mechanisms for minor and trace substitution of H in the nominally anhydrous silicates and oxides that compose the mantle. The dense hydrous magnesium and aluminum silicate phases covered here are listed in Table 1 along with formulae, cell parameters and calculated densities. The dense anhydrous magnesium and aluminum silicate phases covered here are listed in Table 2.

NOMINALLY HYDROUS HIGH-PRESSURE SILICATE PHASES

Compositions of the dense hydrous magnesium silicate (DHMS) phases can be displayed in the magnesia-silica-brucite (MgO-SiO_2-$Mg(OH)_2$) ternary (Fig. 1). Along the anhydrous edge fall periclase (MgO), anhydrous phase B, forsterite and its polymorphs (wadsleyite and ringwoodite), enstatite and its polymorphs (akimotoite, and perovskite-type $MgSiO_3$) and quartz and its polymorphs (coesite, and stishovite). On the brucite-forsterite join lie phase A and the humites (norbergite, chondrodite, humite and clinohumite). Near the brucite-anhydrous phase B join, lie phase B and super-hydrous phase B (Fig. 1).

Table 1. Physical properties of nominally hydrous high pressure silicate phases.

Mineral	Formula	F.W. (g)	S.G.	*a* (Å)	*b* (Å)	*c* (Å)	α (°)	β (°)	γ (°)	Z	MVol (cm^3)	ρ STP (g/cm^3)	References
Brucite	$Mg(OH)_2$	58.327	$P\bar{3}m1$	3.142	3.142	4.766	90	90	120	1	24.54	2.377	Zigan and Rothbauer (1967)
Serpentine	$Mg_3Si_2O_5(OH)_4$	277.137	$P31m$	5.332	5.332	7.223	90	90	120	1	107.24	2.584	Mellini (1982)
Talc	$Mg_3Si_4O_{10}(OH)_2$	379.294	$C\bar{1}$	5.290	9.173	9.460	90.46	98.68	90.09	2	136.63	2.776	Perdikatsis and Burzlaff (1981)
Chlorite	$Mg_5Al_2Si_3O_{10}(OH)_8$	555.838	$C2/m$	5.327	9.227	14.327	90	96.81	90	2	210.540	2.639	Smyth et al. 1997
Mica Group													
Muscovite $2M_1$	$KAl_2AlSi_3O_{10}(OH)_2$	398.317	$C2/c$	5.192	9.015	20.046	90	95.74	90	4	140.546	2.834	Rothbauer (1971)
Phlogopite 1M	$KMg_3AlSi_3O_{10}(OH)_2$	417.290	$C2/m$	5.308	9.190	10.166	90	100.10	90	2	147.012	2.838	Hazen and Burnham (1973)
Phengite $2M_1$	$KMgAlSi_4O_{10}(OH)_2$	396.753	$C2/c$	5.205	9.037	19.886	90	95.62	90	4	140.133	2.831	Smyth et al. (2000)
Amphibole Group													
Cummingtonite	$(Mg,Fe)_7Si_8O_{22}(OH)_2$	843.953	$C2/m$	9.5220	18.1833	5.3184	90	102.020	90	2	271.634	2.879	Yang et al. (1998)
Tremolite	$Ca_2Mg_5Si_8O_{22}(OH)_2$	812.419	$C2/m$	9.863	18.048	5.285	90	104.79	90	2	273.88	2.966	Hawthorne et al. (1976)
Lawsonite	$CaAl_2Si_2O_7(OH)_2{\cdot}H_2O$	314.243	$Ccmm$	8.795	5.847	13.142	90	90	90	4	101.745	3.088	Baur (1978)
Epidote													
Zoisite	$Ca_2Al_3Si_3O_{12}(OH)$	454.366	$Pnma$	16.188	5.550	10.034	90	90	90	4	135.719	3.347	Grevel et al. (2000)
Clinozoisite	$Ca_2Al_3Si_3O_{12}(OH)$	454.366	$P2_1/m$	8.861	5.583	10.141	90	115.46	90	2	136.388	3.331	Pawley et al. (1996)
Epidote	$Ca_2FeAl_2Si_3O_{12}(OH)$	483.232	$P2_1/m$	8.888	5.628	10.152	90	115.38	90	2	138.147	3.497	Gabe et al. (1973)
Humite Group													
Clinohumite	$Mg_9Si_4O_{16}(OH)_2$	621.162	$P2_1/b$	4.741	10.275	13.704	100.1	90	90	2	201.006	3.089	Ross and Crichton (2001)
Chondrodite	$Mg_5Si_2O_8(OH)_2$	339.744	$P2_1/b$	4.7459	10.3480	7.9002	108.70	90	90	2	116.094	2.926	Ross and Crichton (2001)
Phase A	$Mg_7Si_2O_8(OH)_6$	456.398	$P6_3$	7.868	7.868	9.577	90	90	120	2	154.569	2.952	Kagi et al. (2000)
Phase B	$Mg_{12}Si_4O_{19}(OH)_2$	742.096	$P2_1/c$	10.588	14.097	10.073	90	104.1	90	4	219.530	3.380	Finger et al. (1993)
Suphyd. Phase B	$Mg_{10}Si_3O_{14}(OH)_4$	619.403	$Pnnm$	5.089	13.968	8.696	90	90	90	2	186.122	3.327	Pacalo and Parise (1992)
Phase D	$MgSi_2O_4(OH)_2$	178.499	$P\bar{3}1m$	4.745	4.775	4.345	90	90	120	1	59.287	3.010	Yang et al. (1997)
Phase E	$Mg_2SiO_2(OH)_4$	176.739	$R\bar{3}m$	2.967	2.967	13.886	90	90	120	1	73.613	2.401	Shieh et al. (2000)
Phase Egg	$AlSiO_3(OH)$	120.074	$P2_1/n$	7.1441	4.3346	6.9525	90	98.40	90	4	32.066	3.744	Schmidt et al. (1998)
Phase Pi	$Al_3Si_2O_7(OH)_3$	300.137	$P1$	6.0885	7.2832	7.7234	115.71	88.85	92.89	2	92.795	3.234	Wunder et al. (1993)
Topaz-OH	$Al_2SiO_4(OH)_2$	180.063	$Pbnm$	4.7203	8.9207	8.4189	90	90	90	4	53.371	3.373	Northrup et al. (1994)
K-Cymrite	$KAlSi_3O_8\ H_2O$	296.356	$P6/mmm$	5.3348	5.3348	7.7057	90	90	120	1	114.372	2.591	Fasshauer et al. (1997)

Table 2. Physical properties of nominally anhydrous high pressure silicate phases.

Mineral	Formula	F.W. (g)	S.G.	*a* (Å)	*b* (Å)	*c* (Å)	α (°)	β (°)	γ (°)	Z	MVol (cm^3)	ρ STP (g/cm^3)	References
Periclase	MgO	40.311	$Fm\bar{3}m$	4.211	4.211	4.211	90	90	90	4	11.242	3.585	Hazen (1976)
Wüstite	FeO	71.846	$Fm\bar{3}m$	4.311	4.311	4.311	90	90	90	4	12.060	5.956	Hazen (1981)
Corundum	Al_2O_3	101.961	$R\bar{3}c$	4.7589	4.7589	12.9912	90	90	120	6	25.577	3.986	Newnham and DeHaan (1962)
Rutile	TiO_2	79.899	$P4_2/mnm$	4.5845	4.5845	2.9533	90	90	90	2	18.693	4.274	Shintani et al. (1975)
Quartz	SiO_2	60.086	$P3_121$	4.914	4.914	5.405	90	90	120	3	22.685	2.648	Kihara (1990)
Coesite	SiO_2	60.086	$C2/c$	7.137	12.370	7.174	90	119	90	16	20.573	2.920	Smyth et al. (1987)
Stishovite	SiO_2	60.086	$P4_2/mnm$	4.179	4.179	2.665	90	90	90	2	14.014	4.287	Ross et al. (1990)
Olivine													
Forsterite	Mg_2SiO_4	140.709	$Pbnm$	4.753	10.190	5.978	90	90	90	4	43.596	3.227	Smyth et al. (2006)
Fayalite	Fe_2SiO_4	203.779	$Pbnm$	4.820	10.479	6.087	90	90	90	4	46.283	4.402	Fujino et al. (1981)
Wadsleyite	Mg_2SiO_4	140.709	$Imma$	5.711	11.467	8.256	90	90	90	8	40.699	3.457	Finger et al. (1993)
Wadsleyite II	Mg_2SiO_4	140.709	$Imma$	5.6884	28.924	8.2382	90	90	90	20	40.812	3.447	Smyth et al. (2005)
Ringwoodite	Mg_2SiO_4	140.709	$Fd\bar{3}m$	8.092	8.092	8.092	90	90	90	8	39.886	3.527	Smyth et al. (2004)
γ-Fe_2SiO_4	Fe_2SiO_4	203.779	$Fd\bar{3}m$	8.234	8.234	8.234	90	90	90	8	42.023	4.848	Yagi et al. (1974)
Anhyd. Phase B	$Mg_{14}Si_5O_{24}$	864.789	$Pmcb$	5.908	14.241	10.069	90	90	90	2	255.081	3.390	Hazen et al. (1992)
Garnets													
Pyrope	$Mg_3Al_2Si_3O_{12}$	403.153	$Ia\bar{3}d$	11.452	11.452	11.452	90	90	90	8	113.056	3.565	Armbruster et al. (1992)
Almandine	$Fe_3Al_2Si_3O_{12}$	497.758	$Ia\bar{3}d$	11.531	11.531	11.531	90	90	90	8	115.412	4.312	Armbruster et al. (1992)
Majorite	$Mg_3(MgSi)Si_3O_{12}$	401.590	$I4_1/a$	11.501	11.501	11.480	90	90	90	8	114.305	3.513	Angel et al. (1989)
Pyroxenes													
Orthoenstatite	$Mg_2Si_2O_6$	200.795	$Pbca$	18.227	8.819	5.179	90	90	90	8	62.666	3.204	Yang and Ghose (1995)
Orthoferrosilite	$Fe_2Si_2O_6$	263.865	$Pbca$	18.427	9.076	5.237	90	90	90	8	65.930	4.002	Sueno et al. (1976)
Clinoenstatite	$Mg_2Si_2O_6$	200.795	$P2_1/c$	9.618	8.815	5.176	90	108.37	90	4	62.704	3.202	Pannhorst (1984)
Jadeite	$NaAlSi_2O_6$	202.139	$C2/c$	9.423	8.564	5.223	90	107.56	90	4	60.498	3.341	Cameron et al. (1973)
Diopside	$CaMgSi_2O_6$	232.330	$C2/c$	9.750	8.926	5.251	90	105.90	90	4	66.167	3.511	Cameron et al. (1973)
Akimotoite	$Mg_2Si_2O_6$	200.795	$R\bar{3}$	4.728	4.728	13.559	90	90	120	3	52.700	3.810	Horiuchi et al. (1982)
Kyanite	Al_2SiO_5	162.047	$P\bar{1}$	7.126	7.852	5.575	89.99	101.11	106.03	4	44.219	3.664	Winter and Ghose (1979)
Perovskite	$MgSiO_3$	100.397	$Pbnm$	4.775	4.929	6.908	90	90	90	4	24.482	4.100	Horiuchi et al. (1987)
Post-perovskite*	$MgSiO_3$	100.397	$Cmcm$	2.65	8.69	6.59	90	90	90	4	22.89	4.386	Murakami et al. (2004)
Zircon	$ZrSiO_4$	183.304	$I4_1/amd$	6.6042	6.6042	5.9796	90	90	90	4	39.264	4.668	Hazen and Finger (1976)
Titanite	$CaTiSiO_5$	196.063	$P2_1/a$	7.069	8.722	6.566	90	113.86	90	4	55.739	3.517	Kek et al. (1995)

* decompressed from Murakami et al. (2004) assuming K = 300 GPa and K′ = 5

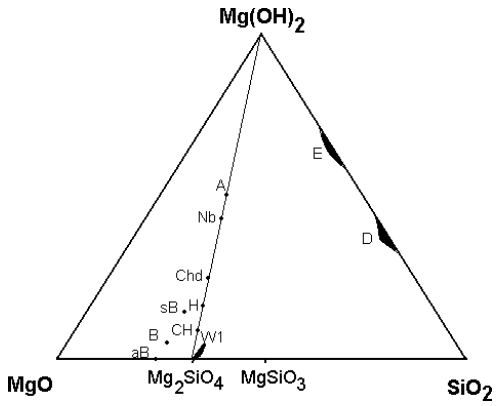

Figure 1. The compositions of the dense, hydrous and anhydrous magnesium silicate phases displayed on the MgO-SiO_2-$Mg(OH)_2$ ternary. W denotes the field for wadsleyite, olivine, and ringwoodite; aB is anhydrous phase B; B is phase B, sB is superhydrous phase B; CH clinohumite; H humite, Chd chondrodite; Nb norbergite; A phase A; E phase E; and D phase D.

Brucite

Brucite, $Mg(OH)_2$ is the first phase discussed among the nominally hydrous minerals of the mantle. Although brucite is not a silicate, it forms a prominent structural component in many silicate minerals. Because of its very high water content, more than 30% by weight or about 75% water by volume, it is not a likely mantle mineral. Brucite forms the most hydrous end member in our systems and is a common ingredient in starting compositions to experimentally produce hydrous high pressure phases. This component, with some Al substitution also occurs in the chlorite structure. The brucite structure (Fig. 2) is trigonal, $P\bar{3}m1$, and consists of tri-octahedral layers of $Mg(OH)_6$ octahedra parallel to (001). All oxygens in the structure are equivalent and protonated, so that each oxygen is bonded to three Mg atoms and one proton. The layers are bonded by relatively weak hydroxyl bonds giving the mineral its perfect basal cleavage. Gibbsite, $Al(OH)_3$, is isostructural with brucite except that one third of the octahedra are vacant.

Serpentine

Serpentine, ideally $Mg_3Si_2O_5(OH)_4$, is a major alteration phase in ultramafic rocks. It is stable at ambient pressure and to depths of roughly 250 km in a cool, subducting slab (Kawamoto et al. 1996; Schmidt and Poli 1998). It contains roughly 13% H_2O by weight which corresponds to more than 30% by volume. The structure consists of a tri-octahedral brucite-like layer attached to a single pure-silica tetrahedral layer (Fig. 3). The structure has several stacking polytypes, but most are similar in composition and density. In its absestiform habit known as chrysotile, the sheets are rolled into tubes, so that the actual space groups and structure are not well defined. Several stacking polytypes have been described with differing degrees of order each having a density of about 2.58 g/cm^3. Lizardite 1H is trigonal $P31m$ (Table 1) (Mellini 1987). The well crystallized massive form is known as antigorite, the space group is triclinic, $P\bar{1}$. There are no Si-OH bonds in the structure, so that each oxygen is bonded either to three Mg and one Si or to three Mg and one proton.

Talc

Talc, $Mg_3Si_4O_{10}(OH)_2$, is also a major alteration phase of mafic rocks. It contains more silica than serpentine and may occur in more siliceous rock compositions than serpentine. The water content is a bit less than 5% by weight. Its triclinic, $C\bar{1}$ structure (Fig. 4) is that of a *T*-O-*T* layer silicate like mica, but without interlayer cations. The bonding between layers is just the weak Van der Waals bonds resulting in a very soft and easily deformable structure. There are no Si-OH bonds in the structure so that one sixth of the oxygen atoms are protonated and bonded to one proton and three Mg atoms. The remaining oxygen atoms are each bonded to one Si and three Mg atoms.

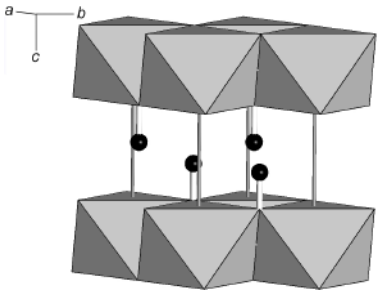

Figure 2. The structure of brucite ($Mg(OH)_2$) is trigonal, $P\bar{3}m1$. All oxygen atoms are equivalent and bonded to one H and three Mg atoms. The Mg octahedra are arranged in a sheet parallel to (001). The sheets are H-bonded together giving the mineral its perfect basal cleavage.

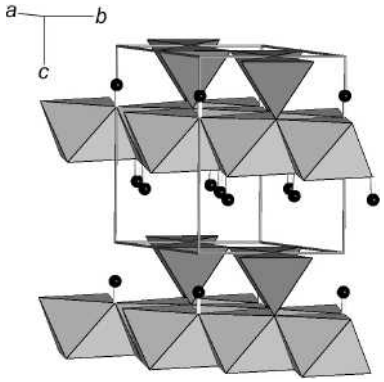

Figure 3. The simple trigonal structure of the serpentine mineral lizardite, $Mg_3Si_2O_5(OH)_4$, is $P31m$. The octahedral Mg atoms are arranged in a trioctahedral sheet as in brucite. All non-silicate oxygens are protonated.

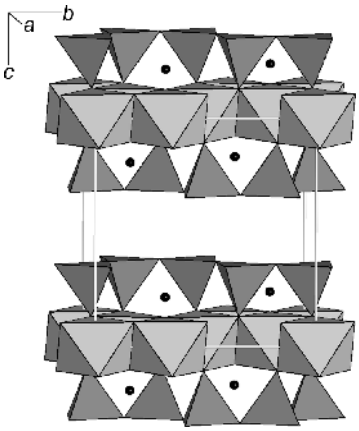

Figure 4. The structure of talc, $Mg_3Si_4O_{10}(OH)_2$, is triclinic, $C\bar{1}$. The octahedral Mg atoms are arranged in a trioctahedral sheet as in brucite and serpentine except tat there are tetrahedral sheets on both sides of the octahedral sheet. Again, all non-silicate oxygens are protonated.

True micas

The true micas (Fig. 5) have a *T*-O-*T* layer like that of talc, but one fourth of the Si cations are replaced by Al and charge balanced by an interlayer alkali cation, dominantly K. Like talc, the micas contain 4.5 to 5% H_2O by weight. In muscovite, $KAl_2AlSi_3O_{10}(OH)_2$, the octahedral layer is dioctahedral with two Al cations, whereas in biotite and phlogopite, $KMg_3AlSi_3O_{10}(OH)_2$, it is trioctahedral with three divalent cations, Mg or Fe, per formula unit. The phengite substitution into the dioctahedral micas puts additional silicon into the tetrahedral layer in place of Al which is charge-balanced by Mg in the dioctahedral layer. This substitution is stabilized by pressure, and high-silica phengites have been synthesized at pressures as high as 11 GPa (Domanik and Holloway 1996; Smyth et al. 2000). Phengite is stable in a mafic composition to over 300 km depth if K is present and temperatures are low as in a subducting slab. The micas exist in several polytypes, that is, different stacking sequences,

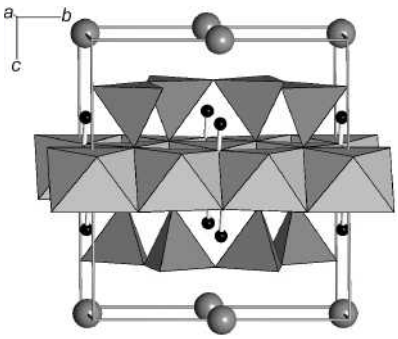

Figure 5. The structure of phlogopite 1M, $KMg_3AlSi_3O_{10}(OH)_2$ is monoclinic *C*2/*m*. One third of the Si atoms in the tetrahedral layer are replaced by Al and charge-balanced by the interlayer K atoms (gray sphere). Muscovite, $KMg_3AlSi_3O_{10}(OH)_2$, is similar except that one third of the octahedra are vacant and the rest replaced by Al. There are several distinct stacking arrangements called polytypes.

predominantly $2M_1$ (*C*2/*c*) and 3T ($P3_112$) in dioctahedral micas, and 1M (*C*2/*m*) and $2M_1$ in trioctahedral micas. The different polytypes commonly coexist in natural samples and are so close in physical properties that separate stability fields for the different polytypes have not been documented. Again, there are no Si-OH bonds and protons coordinate the non-silicate oxygens in the octahedral layer.

The 10 Å phase, $Mg_3Si_4O_{10}(OH)\cdot H_2O$, is a mica-like dense hydrous magnesium silicate phase that occurs at 3-5 GPa as a breakdown product of serpentine and chlorite (Yamamoto and Akimoto 1977). It is structurally similar to talc and phlogopite, but has neutral molecular water in the inter-layer (Fumagalli et al. 2001; Comodi et al. 2005). It is likely to be an important host phase for H in subducting hydrated lithosphere (Fumagalli and Poli 2005).

Chlorite

Chlorite, $Mg_3AlSi_3O_{10}(OH)_2\cdot Mg_2Al(OH)_6$, is another low pressure alteration phase of mafic and ultramafic rocks. Like talc, it is stable to about 100 km depth, but is distinct from talc in its Al-content. The structure (Fig. 6) is monoclinic *C*2/*m* or triclinic, $C\bar{1}$, and consists of trioctahedral talc-like layer, but with one fourth of the tetrahedral sites occupied by Al instead of Si, giving the layer a net negative charge. Instead of an interlayer cation as in micas, there is a trioctahedral brucite-like layer with one third of the octahedra occupied by Al instead of Mg giving the layer a net positive charge. In the brucite-like layer, all of the oxygen atoms are protonated, whereas in the talc-like later one-sixth of the oxygens are protonated. Again, there are no Si-OH bonds in the structure. Chlorite, like serpentine, contains about 13% H_2O by weight.

Amphiboles

The amphiboles $A_{0\text{-}1}X_7Y_8O_{22}(OH)_2$, are complex hydrous chain silicate minerals of high grade metamorphic and igneous rocks in which *A* is an alkali cation, *X* an octahedral divalent or trivalent cation, and *Y* is tetrahedral Si or Al. The structure (Fig. 7) is based on a double tetrahedral chain parallel to *c*. Again, there are no Si-OH bonds and all non-silicate oxygens (one in 12) are protonated. Amphiboles are stable in subducting lithosphere to about 3 GPa (Kawamoto et al. 1996; Schmidt and Poli 1998), so they are not expected to be major hosts for H in the sub-lithospheric mantle. Amphibole-like double chain defects are relatively common in pyroxenes at low pressures and so may be a water-carrying defect in mantle pyroxenes.

Lawsonite

Lawsonite, $CaAl_2Si_2O_7(OH)_2\cdot H_2O$, contains molecular water as well as hydroxyl. The structure (Fig. 8) is orthorhombic, *Ccmm*, and is a sorosilicate with Si_2O_7 groups, Al in octahedral coordination, and Ca in 8-coordination. Again, there are no Si-OH bonds, and the two of the non-silicate oxygen atoms coordinating Al are hydroxyls, and two of the oxygens coordinating Ca are water molecules. Lawsonite is a common hydrous alteration product of mafic igneous rocks, replacing calcic plagioclase feldspar. The total water content of lawsonite

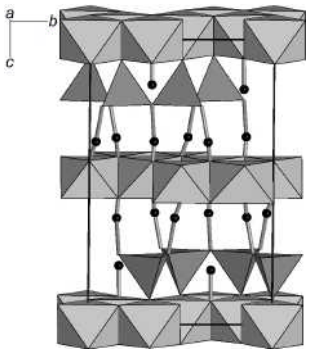

Figure 6. The structure of chlorite, $Mg_3AlSi_3O_{10}(OH)_2\ Mg_2Al(OH)_6$ is monoclinic, *C*2/*m*, or triclinic, $C\bar{1}$. There are talc-like layers interspersed with brucite-like layers. One third of the Si atoms are replaced by Al giving the talc layer a net negative charge, and one third of the Mg atoms in the brucite-like layer are replaced by Al to give that layer a net positive charge. There are no Si-O-H bonds and all non silicate oxygens are protonated.

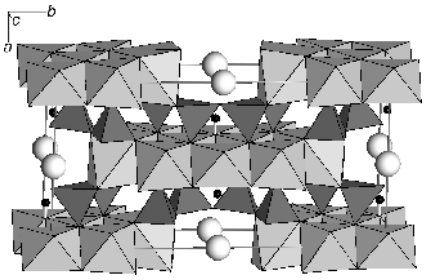

Figure 7. The structure of the amphibole tremolite, $Ca_2Mg_5Si_8O_{22}(OH)_2$, is monoclinic *C*2/*m*. The only non-silicate oxygen is protonated (black).

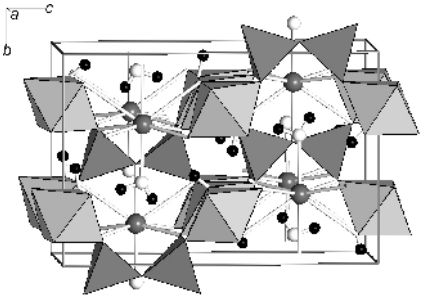

Figure 8. The structure of lawsonite, $CaAl_2Si_2O_7(OH)_2{\cdot}H_2O$ is orthorhombic, *Ccmm*. Lawsonite is a sorosilicate containing Si_2O_7 groups. The structure contains molecular water as well as hydroxyl. The Ca atom (gray sphere) is 8-coordinated, whereas the Al is octahedral, and the Si tetrahedral.

is high at about 11.5% by weight, and it is stable to relatively high pressures (~10 GPa) and low temperatures (Pawley 1994). Despite its high water content, it is about 10% denser than anorthite, and relatively incompressible with an isothermal bulk modulus of 122 GPa (Boffa-Balaran and Angel 2003). Being stable to depths of 300 km in the crustal portion of a subducting slab, lawsonite may act as a major conduit for water in the crustal portion of the slab to depths approaching those of the transition zone.

Epidote

The epidote group comprises epidote ($Ca_2(Al,Fe)_3Si_3O_{12}(OH)$), zoisite, and clinozoisite ($Ca_2Al_3Si_3O_{12}(OH)$). Epidote is a very common metamorphic alteration product of mafic igneous rocks, whereas zoisite and clinozoisite are more restricted in composition and occurrence to aluminous and peraluminous rocks. The pressure stability ranges from less than 0.1 GPa to near 7 GPa (Poli and Schmidt 2004). There are also Mn-rich varieties (piemontite), and rare-earth-rich (allanite) varieties as well as several more named chemical variants (Franz and Liebscher 2004). The structure (Fig. 9) is monoclinic, $P2_1/m$ ($Z = 2$), and has both isolated SiO_4 tetrahedra as well as Si_2O_7 groups, so it is classed as a sorosilicate. Zoisite is orthorhombic, *Pnma,* with a nearly identical structure, but twice the unit cell volume ($Z = 4$). Most of the iron

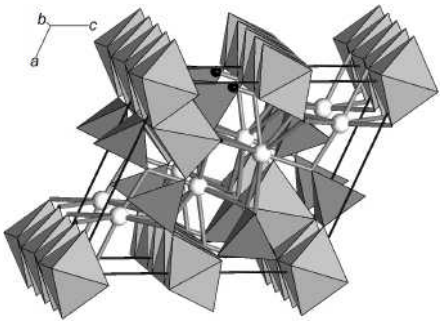

Figure 9. The structure of epidote, $CaAl_2FeSi_3O_{12}(OH)$, and clinozoisite, $CaAl_3Si_3O_{12}(OH)$, is monoclinic $P2_1/m$. The only non-silicate oxygen has a proton (black).

is ferric, and epidote has all of its trivalent cations in octahedral coordination, so it is also denser than anorthite. The O10 position is a non-silicate oxygen and is protonated. There is another non-silicate oxygen, O4, which is bonded to three trivalent metal octahedra. This oxygen is not protonated directly but shares a longer hydrogen bond to the proton on O10.

Humite

The humite group comprises norbergite ($Mg_3SiO_4(F,OH)_2$), chondrodite ($Mg_5Si_2O_8(F,OH)_2$), humite ($Mg_7Si_3O_{12}(F,OH)_2$), and clinohumite ($Mg_9Si_4O_{16}(F,OH)_2$). Humites are relatively rare components of hydrothermally altered ultramafic rocks. They also occur in other silica-undersaturated rocks such as skarns and carbonatites. Natural humites almost always contain more F than hydroxyl. All of the humites lie on the join forsterite-brucite (Fig. 1). The formulas can be thought of as $n{\cdot}(Mg_2SiO_4){\cdot}Mg(OH)_2$ where n is one for norbergite, two for chondrodite, three for humite, and four for clinohumite, so that all have a higher (Mg+Fe)/Si ratio than does olivine. Because of this they are not thought to be major hydrous components of the mantle, which is generally considered to have a lower (Mg+Fe)/Si ratio than olivine. The F-free pure Mg clinohumite and chondrodite are stable to pressures greater than 14 GPa and temperatures greater than 1250 °C, but are not known to coexist with enstatite. The structures of chondrodite and clinohumite are illustrated in Figures 10 and 11. Although humite and norbergite have not been reported from pressure higher than about 3 GPa, hydroxy-chondrodite and hydroxy-clinohumite are stable at pressures and temperatures well into the transition zone (Yamamoto and Akimoto 1977; Burnley and Navrotsky 1996; Wunder 1998).

Clinohumite

Clinohumite ($Mg_9Si_4O_{16}(OH)_2$) can coexist with chondrodite or with olivine at high pressure but not with phase A or enstatite (Fig. 1). The structure (Fig. 10) is monoclinic, $P2_1/b$ (a-unique). The odd setting of the space group is chosen to preserve the olivine axial relation (Table 1). The c-axis is greater than that of chondrodite by approximately 6 Å, and the α-angle is reduced to about 100°. Hydroxy-clinohumite has the problem of protonating two identical oxygens symmetrically disposed about the inversion (Friedrich et al. 2001). But again, there are no Si-OH bonds and all non-silicate oxygens are protonated in pure hydroxy-clinohumite. Berry and James (2001) report a second partially occupied deuteron position in pure hydroxyl clinohumite located on the hydroxyl oxygen approximately 180° away from the position near the inversion on the O9-O9 edge.

Chondrite

Chondrodite ($Mg_5Si_2O_8(OH)_2$) can coexist with phase A or with hydroxy-clinohumite at pressures to about 14 GPa. Its structure (Fig 11) resembles olivine with a and b axes nearly the same as olivine, but c different and the space group is monoclinic, $P2_1/b$. The O5 is the only non-silicate oxygen and is protonated. As with clinohumite, there is a problem with protonation

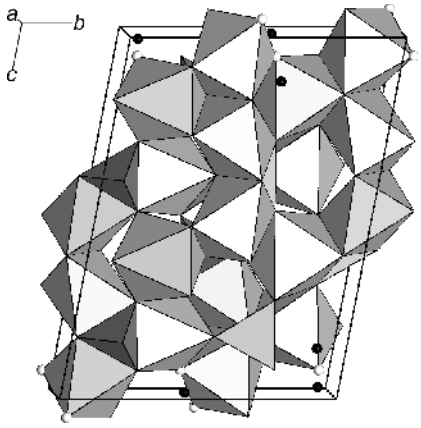

Figure 10. The structure of clinohumite, $Mg_9Si_4O_{16}(OH)_2$, is monoclinic $P2_1/b$. The odd setting of the space group is chosen to maintain the structural relation to olivine.

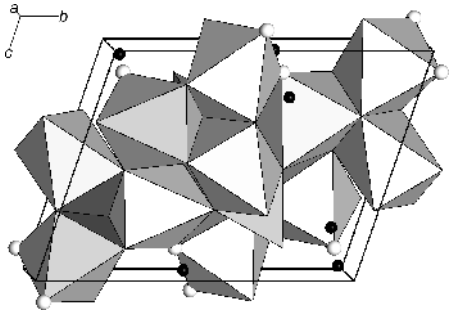

Figure 11. The structure of chondrodite, $Mg_5Si_2O_8(OH)_2$, is monoclinic $P2_1/b$. The odd setting of the space group is chosen to maintain the structural relation to olivine.

of every O5 in that this position is close to the inversion center and putting the proton on the O5-O5 edge would put the protons too close to each other. For synthetic deuterated chondrodite ($Mg_5Si_2O_8(OD)_2$), Lager et al. (2001) identified a second partially occupied deuteron position located approximately 180° away from the primary deuteron position on O5. Again, there are no Si-OH bonds and all non-silicate oxygens are protonated in pure hydroxy-chondrodite.

Phase A

Phase A ($Mg_7Si_2O_8(OH)_6$) is stable under very hydrous conditions at pressures of 3 to about 8 GPa and temperatures of 550 to about 1250 °C (Yamamoto and Akimoto 1977). The structure (Fig. 12) is hexagonal, $P6_3$, and consists of slightly distorted close-packed layers of oxygen atoms and hydroxyl groups repeating along the *c*-axis in an ABCB sequence (Horiuchi et al. 1979). This contrasts with the hexagonal close-packed sequence of ABAB in olivine and the humites. Mg occupies one special position on the 3-fold axis (*M*3) and two general positions, *M*1 and *M*2. Si occupies two special positions, one each on the 3-fold and on the 6_3 axes, so that there is one in each layer of cations. All tetrahedra point in the same direction along *c,* so that the structure is acentric. The O2 and O4 oxygen sites are hydroxyls (Kagi et al. 2000), so all non-silicate oxygens are protonated and there are no Si-OH bonds in the structure. The density is relatively low (2.95 g/cm^3) consistent with its high water content (~12% by weight) and limited pressure stability range. Phase A is a possible phase in the mantle as a breakdown product of serpentine, and may coexist with brucite or chondrodite, but probably not with olivine (Luth 1995).

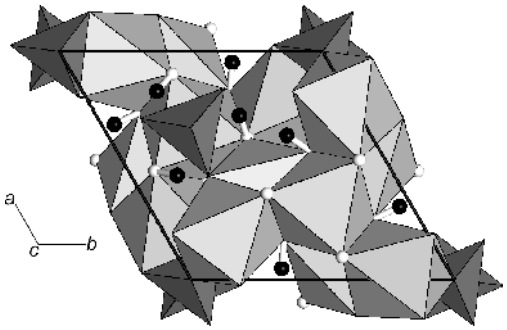

Figure 12. The structure of Phase A, $Mg_7Si_2O_8(OH)_6$, is acentric hexagonal, $P6_3$.

Phase B

Phase B ($Mg_{12}Si_4O_{19}(OH)_2$) along with superhydrous phase B (SHyB) and anhydrous phase B (AHyB), contains Si in both octahedral and tetrahedral coordination and has a Mg/Si ration greater than two (Finger et al. 1989). Phase B is stable under pressure and temperature conditions of the Transition Zone. The density is greater that that of forsterite, but less than that of wadsleyite or ringwoodite, despite the presence of octahedral silicon. The structure (Fig. 13) is monoclinic, $P2_1/c$, and all atoms except $M1$ and $M3$ are in general positions. There are four Si sites, three of which are tetrahedral and one octahedral. There are 13 distinct Mg octahedral sites and 21 distinct oxygen sites of which two are hydroxyls. All non-silicate oxygens are protonated and there are no Si-OH bonds in the structure.

Superhydrous Phase B

Superhydrous Phase B ($Mg_{10}Si_3O_{14}(OH)_4$) (SHyB) is similar to phase B in having both octahedral and tetrahedral silicon, a stability range within the transition zone, and a Mg/Si ratio greater than two. The density is slightly less than that of phase B. The structure (Fig. 14) is orthorhombic, *Pnnm* (Pacalo and Parise 1992), and half of the Si atoms are octahedral and half tetrahedral. There are four distinct Mg octahedra and six oxygen sites. Although all non-silicate oxygens are protonated and there are no Si-OH bonds in the structure, one of the silicate oxygens is under-bonded (O3) and one is over bonded (O6) which leads to the distortions of the coordination polyhedra. As with the other B-phases, its Mg/Si ratio is greater than two, so it is not a likely phase in an enstatite or majorite bearing mantle assemblage. Koch-Müller et al. (2005) report polymorphic inversion in superhydrous phase B with an ordered low temperature polymorph having symmetry *Pnn*2. The reduction in symmetry with ordering causes splitting of the Mg positions, but not the Si positions.

Phase D

Phase D ($MgSi_2O_4(OH)_2$) is stable into the lower mantle at pressures of 17 to 50 GPa (Frost and Fei 1999) and has both Mg and Si in octahedral coordination (Fig. 15). The structure is

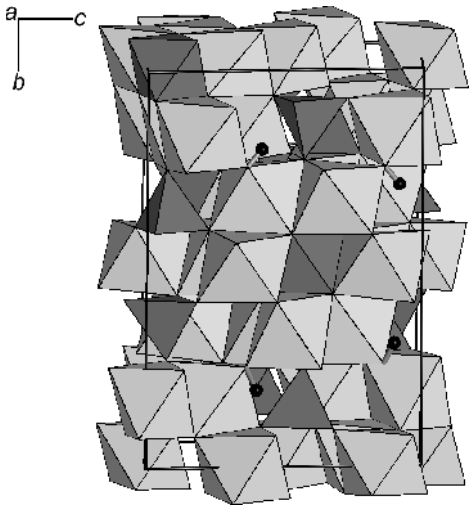

Figure 13. The structure of Phase B, $Mg_{12}Si_4O_{19}(OH)_2$, is monoclinic, $P2_1/c$.

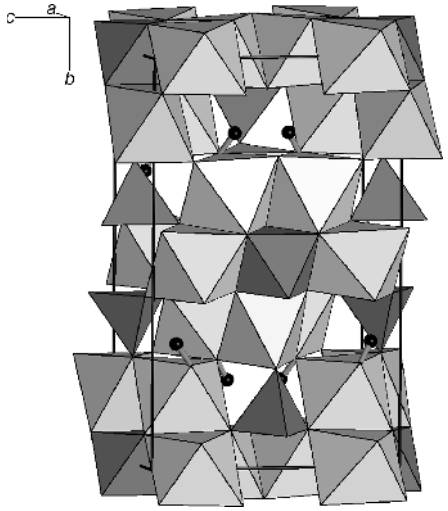

Figure 14. The structure of superhydrous Phase B (ShyB), $Mg_{10}Si_3O_{14}(OH)_4$, is orthorhombic, *Pnnm*.

highly disordered with variable Mg/Si ratios and water contents ranging from 10 to 18% by weight (Yang et al. 1997). The density of the ideal trigonal structure ($P\bar{3}1m$) is about 3.01 g/cm^3. All oxygens are equivalent and bonded to two Si, one Mg, and one proton, although only about one third of the proton positions can be occupied. Although the density is only about 75% that of the lower-mantle anhydrous assemblage, phase D is the likely host phase for H in the lower mantle.

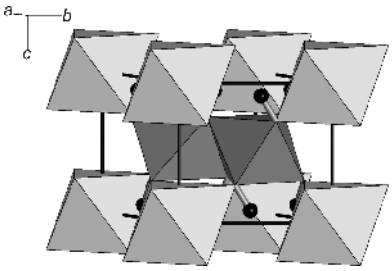

Figure 15. The structure of Phase D, $MgSi_2O_4(OH)_2$, is trigonal, $P\bar{3}1m$.

Phase E

Phase E ($Mg_2SiO_2(OH)_4$) is a highly disordered structure with Si in tetrahedral and Mg in octahedral coordination. The structure (Fig. 16) is trigonal $R\bar{3}m$ with variable Mg/Si ratio and H content (Kudoh et al. 1993). In the structure the *M*2 site occurs in an octahedral site adjacent to the Si tetrahedron, so that either one or the other can be occupied but not both. There is no long range order and charge balance is made up by protonation. The structure occurs in very hydrous compositions as a breakdown product of serpentine at pressures of 13 to 17 GPa and temperatures of 800 to 1300 °C (Kanzaki 1991).

Phase Pi

Phase Pi ($Al_3Si_2O_7(OH)_3$) is so called because was formerly thought to be the poorly described synthetic mineral piezotite (Coes 1962). The mineral has been synthesized at low temperatures and moderate pressures (500-650 °C and 4-5.5 GPa) (Wunder et al. 1993) in the hydrous aluminosilicate system. The structure (Fig. 17), is acentric triclinic, *P*1, with Al in octahedral and Si in tetrahedral coordination (Daniels and Wunder 1993, 1996). There are 20 distinct oxygen atoms in the unit cell, of which six should be hydroxyls if the formula is correct. Four of the oxygens (O9, O10, O19, O20) are bonded to just two Al atoms and so

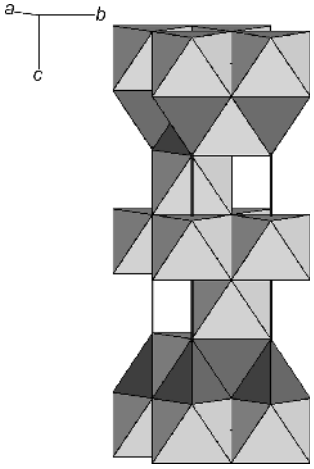

Figure 16. The structure of Phase E, $Mg_2SiO_2(OH)_4$ is trigonal $R\bar{3}m$. The structure is highly disordered. The silicate layer (dark) can have tetrahedral voids occupied by Si or octahedral voids occupied by Mg.

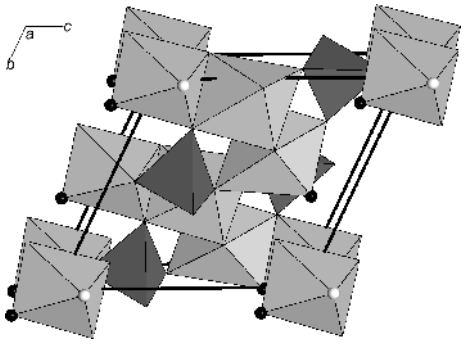

Figure 17. The structure of phase Pi ($Al_3Si_2O_7(OH)_3$) is acentric, triclinic P1. Although the proton positions have not been determined for this phase, the oxygen atoms shown as black spheres are protonated non-silicate oxygens. The remaining two underbonded oxygens shown as white spheres are likely protonated silicate oxygen atoms.

are certainly hydroxyls. The remaining oxygens all bond to Si. Of these, O4 and O14 bond to one Si and one Al, and so are also underbonded. They each have very long Al-O distances so are apparently hydroxyls, but unusual in that they may be protonated silicate oxygens.

Topaz-OH

Topaz-OH ($Al_2SiO_4(OH)_2$) also occurs in the hydrous aluminosilicate system at temperatures of 600-1000 °C and pressures up to about 12 GPa (Pawley 1994; Schmidt et al. 1998; Wunder et al. 1999). The structure (Fig. 18) is orthorhombic, *Pbnm*, with Al in octahedral and Si in tetrahedral coordination. The structure is relatively dense (3.37 g/cm^3), more dense than phase Pi, but less dense than phase Egg or kyanite. Curiously, it is significantly less dense than fluoro-topaz. This may be because the protons are disordered over two distinct positions (Northrup et al. 1994).

Phase Egg

Phase Egg $AlSiO_3(OH)$ is named after the first author to describe the phase (Eggleton 1978) and has a 1:1 Al:Si ratio. It occurs at pressure ranges into the transition zone at 11-18 GPa and temperatures of 700-1300 °C as a high pressure breakdown product of hydroxyl-topaz. The structure was solved and proton positions located to high precision by neutron powder diffraction (Schmidt et al. 1998). The structure is monoclinic, $P2_1/n$, and has both Si and Al in octahedral coordination (Fig. 19). There are four distinct oxygens in the structure. The O1 and O2 oxygens are bonded to two Si and one Al positions, whereas O4 is the hydroxyl, but it is also bonded to two Al and one Si, as is O3. The long H bond extends to O3. With octahedral silica and a single hydroxyl, the structure is relatively incompressible with a bulk modulus of 157 GPa and K′ of 6.5 (Vanpeteghem et al. 2003).

K-cymrite

K-cymrite ($KAlSi_3O_8{\cdot}H_2O$) occurs as a hydration product of sanidine at pressures above 3GPa and temperatures of 350-750 °C. It is isostructural with cymrite ($BaAl_2Si_2O_8{\cdot}H_2O$) and has a layered structure of a double tetrahedral sheet (Fig. 20) with molecular water within the layer and K between the sheets (Fasshauer et al. 1997). The symmetry is *P6/mmm* so that the tetrahedral Al and Si are disordered over the sheet. There are bridging

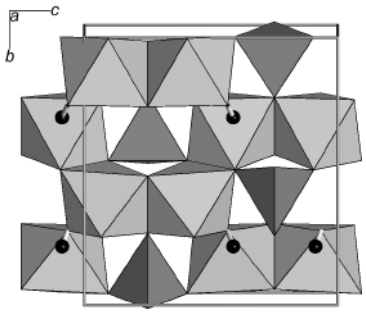

Figure 18. The structure of topaz-OH, $Al_2SiO_4(OH)_2$ is orthorhombic *Pbnm*. Despite its stability to quite high pressures (~12 GPa) it is significantly less dense at zero pressure than fluorotopaz.

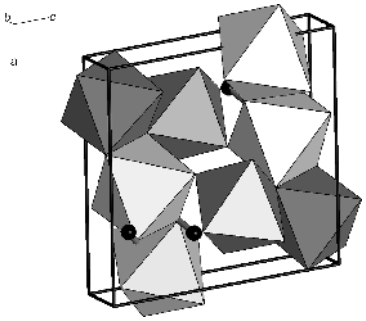

Figure 19. The structure of Phase Egg, $AlSiO_3(OH)$, is monoclinic $P2_1/n$. It has both Al (light) and Si (dark) in octahedral coordination.

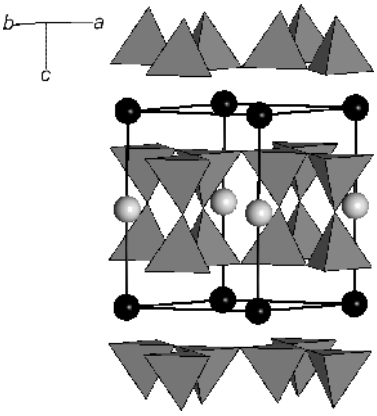

Figure 20. The structure of K-cymrite ($KAlSi_3O_8{\cdot}H_2O$) is hexagonal $P6_3/mmm$ and is composed of a double hexagonal layer of disordered Al-Si tetrahedra. K atoms (black) form the interlayer, and molecular water (gray) is in the tetrahedral layer.

oxygens, non-bridging silicate oxygens, as well as molecular water, which lies within the tetrahedral layer (Fig. 20). The proton positions have not been determined, but are likely to be locally determined by the Al occupancy of the nearest tetrahedra. None of the silicate oxygens are protonated. K-cymrite is slightly denser than sanidine (Table 1).

NOMINALLY ANHYDROUS HIGH-PRESSURE SILICATE AND OXIDE PHASES

Periclase-wüstite

Periclase-wüstite ((Mg,Fe)O) is isometric, $Fm\bar{3}m$, with the rock-salt structure (Fig. 21). Pure MgO is stable at low pressures and not known to undergo any high pressure phase transformations, whereas wüstite (FeO) is known to undergo a rhombohedral distortion of this structure at pressures above 20 GPa (Shu et al. 1998; Jacobsen et al. 2005). At low to modest pressures the structure can accommodate significant ferric iron in tetrahedral voids associated with octahedral vacancies. The oxygen site potentials of the nominally anhydrous mantle phases are given in Table 3. Periclase and wüstite have some of the shallowest oxygen potentials of any mantle minerals, which make these phases likely hosts for H if charge balance can be achieved. Murakami et al. (2002) report up to 2000 ppmw H_2O in (Mg,Fe)O ferro-periclase synthesized from a hydrous peridotite composition at 25.5 GPa and 1650 °C. However their FTIR spectra show pleochroism unexpected for a cubic phase raising the possibility of an included hydrous phase of power symmetry. Bolfan Casanova et al. (2000) report only about 2 ppmw H_2O in periclase at 24 GPa and 1500 °C in a pure MgO-SiO_2-H_2O system. Bolfan-Casanova et al. (2003) also report very low H contents in ferro-periclase up to 10 Gpa, so it appears that H_2O solubility in pure MgO and in ferro-periclase of possible lower mantle composition is quite limited.

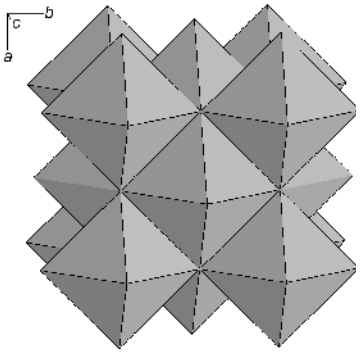

Figure 21. The structure of periclase (MgO) and wüstite (FeO) is the cubic rock salt structure, $Fm\bar{3}m$.

Corundum

Corundum (Al_2O_3) (Fig. 22) is rhombohedral, $R\bar{3}c$, and isostructural with hematite (Fe_2O_3), eskolaite (Cr_2O_3), karelianite (V_2O_3), and synthetic Ti_2O_3. Ilmenite ($FeTiO_3$) and akimotoite ($MgSiO_3$) are also closely related structures with subgroup symmetry, $R\bar{3}$. Natural corundum has not been reported with appreciable H contents, but it is not a common mineral in high pressure assemblages. It occurs in high grade peraluminous rocks with zoisite or in peraluminous eclogites. Rossman and Smyth (1990) report no observable OH stretch features in the FTIR spectrum of a natural corundum from a

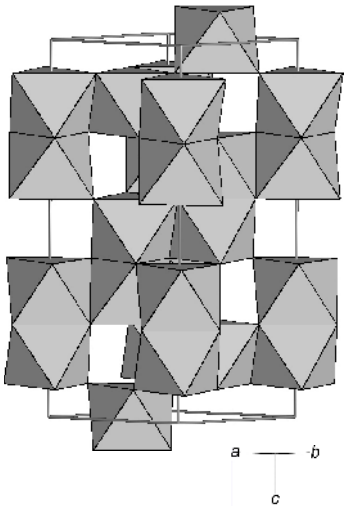

Figure 22 The structure of corundum (Al_2O_3) and hematite (Fe_2O_3) is trigonal, $R\bar{3}c$.

Table 3. Cation coordinations and electrostatic potentials of oxygen sites in high pressure silicate and oxide phases.

Mineral	Formula	Site	Coordination	Potential (V)
Periclase	MgO	O	6Mg	23.92
Wüstite	FeO	O	6Fe	23.36
Corundum	Al_2O_3	O	4Al	26.40
Rutile	TiO_2	O	3Ti	25.94
Quartz	SiO_2	O	2Si	30.82
Coesite	SiO_2	O1	2Si	29.07
		O2	2Si	29.64
		O3	2Si	30.67
		O4	2Si	30.41
		O5	2Si	30.97
Stishovite	SiO_2	O	3Si	28.61
Olivine				
Forsterite	Mg_2SiO_4	O1	3Mg,1Si	27.69
		O2	3Mg,1Si	27.53
		O3	3Mg,1Si	26.35
Fayalite	Fe_2SiO_4	O1	3Fe,1Si	27.38
		O2	3Fe,1Si	27.20
		O3	3Fe,1Si	26.12
Wadsleyite	Mg_2SiO_4	O1	5Mg	21.28
		O2	1Mg,2Si	30.94
		O3	3Mg,1Si	26.78
		O4	3Mg,1Si	26.97
Wadsleyite II	Mg_2SiO_4	O1	3Mg,1Si	26.83
		O2	5Mg	20.03
		O3	3Mg,1Si	26.41
		O4	3Mg,1Si	26.68
		O5	3Mg,1Si	26.71
		O6	3Mg,1Si	27.34
		O7	1Mg,2Si	30.51
		O8	3Mg,1Si	27.50
Ringwoodite	Mg_2SiO_4	O	3Mg,1Si	26.57
γ-Fe_2SiO_4	Fe_2SiO_4	O	3Fe,1Si	26.28
Anhyd. Phase B	$Mg_{14}Si_5O_{24}$	O1	3Mg,1Si^{IV}	27.09
		O2	4Mg,1Si^{VI}	25.62
		O3	3Mg,1Si^{IV}	26.32
		O4	6Mg	22.70
		O5	3Mg,1Si^{IV}	28.77
		O6	3Mg,1Si^{IV}	27.84
		O7	3Mg,1Si^{IV}	26.66
		O8	4Mg,1Si^{VI}	25.09
		O9	3Mg,1Si^{IV}	26.91
Garnets				
Pyrope	$Mg_3Al_2Si_3O_{12}$	O	4Mg,1Al,1Si	27.06
Almandine	$Fe_3Al_2Si_3O_{12}$	O	4Fe,1Al,1Si	27.08

Mineral	Formula	Site	Coordination	Potential (V)
Pyroxenes				
Orthoenstatite	$Mg_2Si_2O_6$	O1a	3Mg,1Si	26.22
		O2a	2Mg,1Si	26.38
		O3a	1Mg,2Si	30.89
		O1b	3Mg,1Si	26.39
		O2b	2Mg,1Si	26.48
		O3b	1Mg,2Si	30.57
Mg-Tschermaks	$MgAlAlSiO_6$	O1a	1Mg,2Al,1Si	32.09
		O2a	1Mg,1Al,1Si	30.25
		O3a	1Mg,2Si	32.49
		O1b	3Al,1Mg	24.59
		O2b	2Al,1Mg	22.39
		O3b	2Al	21.99
Clinoenstatite	$Mg_2Si_2O_6$	O1a	3Mg,1Si	26.33
		O2a	2Mg,1Si	26.34
		O3a	1Mg,2Si	30.90
		O1b	3Mg,1Si	26.39
		O2b	2Mg,1Si	26.34
		O3b	1Mg,2Si	30.59
Jadeite	$NaAlSi_2O_6$	O1	1Na,2Al,1Si	27.54
		O2	1Na,1Al,1Si	27.15
		O3	2Na,2Si	30.34
Diopside	$CaMgSi_2O_6$	O1	1Ca,2Mg,1Si	25.53
		O2	1Ca,1Mg,1Si	25.78
		O3	2Ca,2Si	30.74
Akimotoite	$Mg_2Si_2O_6$	O	2Mg, 2Si^{VI}	27.38
Kyanite	Al_2SiO_5	O1	2Al,1Si	28.60
		O2	4Al	25.91
		O3	2Al,1Si	27.73
		O4	2Al,1Si	28.01
		O5	2Al,1Si	28.60
		O6	4Al	25.81
		O7	2Al,1Si	27.70
		O8	2Al,1Si	27.97
		O9	2Al,1Si	28.28
		O10	2Al,1Si	28.36
Perovskite	$MgSiO_3$	O1	2Mg,2Si^{VI}	26.91
		O2	3Mg,2Si^{VI}	26.86
Post-perovskite*	$MgSiO_3$	O1	2Mg,2Si^{VI}	27.76
		O2	3Mg,2Si^{VI}	26.77
Zircon	$ZrSiO_4$	O	2Zr,1Si	31.49
Titanite	$CaTiSiO_5$	O1	1Ca,2Ti	24.89
		O2a	1Ca,1Ti,1Si	26.86
		O2b	1Ca,1Ti,1Si	26.96
		O3a	2Ca,1Ti,1Si	26.98
		O3b	2Ca,1Ti,1Si	26.87

high pressure corundum-kyanite eclogite. There is a single oxygen site in the structure. The site potential is significantly deeper than that of periclase but might allow minor protonation if charge balance can be achieved. However, significant protonation of the isostructural akimotoite ($MgSiO_3$) does occur as discussed below.

Coesite

Coesite (SiO_2) is the high pressure polymorph of SiO_2 stable between about 3 and 8 GPa. The structure (Fig. 23) is a relatively dense tetrahedral framework with monoclinic *C*2/*c* symmetry. Natural coesite is normally quite pure SiO_2 with only trace levels of other elements. All oxygens are bridging oxygens bonded only to two Si atoms. There are five distinct oxygen sites in the structure, all with deep potentials similar to quartz (Table 3). Of these O1 has the shallowest potential and the most likely one to be protonated if there were a small amount of B or Al substitution in the tetrahedra. Rossman and Smyth (1990) report no observable OH in a natural coesite in a relatively hydrous coesite-kyanite eclogite. Koch-Mueller et al. (2001) and Mosenfelder (2000) however report up to 200 ppmw H_2O in coesite synthesized at pressures of 7.5 GPa and 1100 °C, but undetectable amounts in coesite synthesized at pressures below 5 GPa. Koch-Müller et al. (2003) report that the major substitution mechanism in coesite is by the hydrogarnet-type (H_4O_4) with relatively minor amounts of H being associated with B and Al substitution. In a low-symmetry tetrahedral framework structure such as coesite, any Si vacancy would result in protonation of the terminating oxygens, but there would be nothing to constrain these oxygens to maintain a tetrahedral configuration, as there is in garnet. Koch-Müller et al. (2001) propose several possible proton locations for coesite on the oxygens coordinating a vacant Si2 position consistent with O-H dipoles observed in polarized infrared spectra. They further suggest that vacancy at Si1 is unlikely because of difficulty in accounting for the pleochroism of one of the major O-H vibrations.

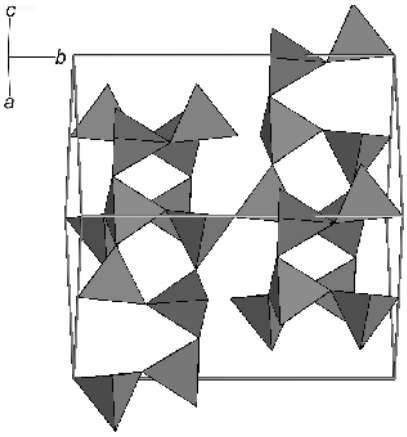

Figure 23. The structure of coesite, SiO_2, is monoclinic *C*2/*c*. All oxygens are bridging oxygens bonded to two tetrahedral Si atoms. Trace hydration of this structure has only been observed in samples quenched from pressures above 5 GPa.

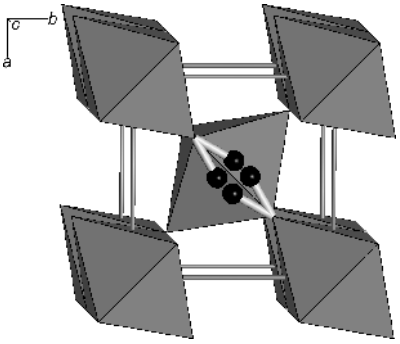

Figure 24. The structure of stishovite (SiO_2) and rutile (TiO_2) is tetragonal, $P4_2/mnm$. All oxygens are equivalent. Protonation of these compounds can accompany trivalent ion substitution in the octahedra. Proton positions determined by neutron single crystal diffraction for rutile (Swope et al. 1995) are illustrated.

Stishovite and rutile

Stishovite (SiO_2) and rutile (TiO_2) (Fig. 24) are isostructural and both may incorporate considerably more H than either coesite or quartz. The stishovite structure is tetragonal $P4_2/mnm$ with all cations in octahedral coordination, and the octahedra share edges in the *c*-direction. All oxygens in the structure are equivalent, and protonation of the oxygens can accompany Al for Si substitution in the octahedra (Smyth et al.

1995). The oxygen site potential is substantially lower than those of quartz or coesite (Table 3). Bolfan-Casanova et al. (2000) report up to 72 ppmw H_2O in stishovite in an Al-free system.

Vlassopoulos et al. (1993) report up to 8000 ppmw H_2O in natural rutile containing minor amounts of trivalent cations (Cr, Fe, V, Al). Principal rutile absorptions in the OH range are at 3290 and 3365 cm^{-1} (Rossman and Smyth 1990; Vlassopoulos et al. 1993) and are strongly polarized normal to the *c*-axis. Swope et al. (1995) report a proton position on the shared octahedral edge for hydrous rutile at $x/a = 0.4176$; $y/b = .5033$, and $z/c = 0$, based on neutron single crystal diffraction of a natural sample. This position is consistent with the strong IR pleochroism and is illustrated in Figure 24.

Pyroxenes

Pyroxenes of major importance to mantle dynamics include enstatite ($Mg_2Si_2O_6$), diopside ($CaMgSi_2O_6$), and jadeite ($NaAlSi_2O_6$), which are all significant components of the upper mantle. For a recent review of pyroxene structures at temperature and pressure see Yang and Prewitt (2000). Enstatite is an orthopyroxene, orthorhombic, *Pbca* (Fig. 25), at pressures to about 7 GPa, whereas enstatite quenched from higher pressures is monoclinic $P2_1/c$. Clinoenstatite transforms to majorite garnet at about 15 GPa, in a pyrolite composition and gradually dissolves into the garnet phase through the upper Transition Zone. Mantle peridotites and lherzolites contain up to about 15 modal percent clinopyroxene that is typically a Cr-diopside with very minor amounts of Na, Al or Fe^{3+}. In eclogites, however, diopside and jadeite form a complete crystalline solution known as omphacite, which is monoclinic *C*2/*c* at high temperatures. Omphacite composes 50% or more of eclogites that form from subducting basalt at pressures of 3 to 13 GPa. Eclogites are quite distinct from peridotites and lherzolites, so that rocks of intermediate composition are virtually unknown among rocks of high pressure origin.

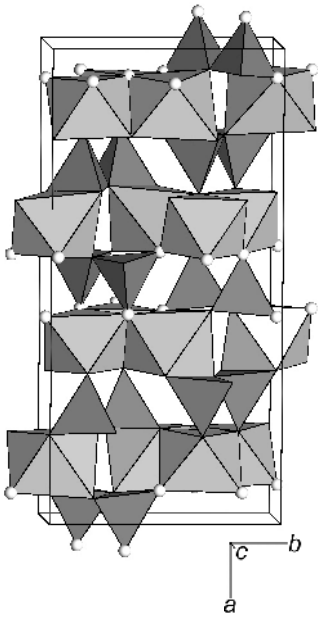

Figure 25. The structure of orthoenstatite, $Mg_2Si_2O_6$, is orthorhombic *Pbca*. This view down *c* with *a*-vertical, shows the alternating layers of T1 and T2 tetrahedra. The likely sites of protonation are on the O2b and O1b oxygens (spheres) with the O-H vectors lying in the *b*-*c* plane.

Orthoenstatite can be a major host for water in the shallow (lithospheric) upper mantle. Rauch and Keppler (2002) report that the solubility of H_2O in enstatite increases to a maximum of about 850 ppmw at 1100 °C at 7.5 GPa and decreases slightly at higher pressures in the clinoenstatite field. In pure Mg enstatite, the strongest OH absorptions in the infrared spectra are polarized parallel to *c*. However, Al has a dramatic effect on the water solubility and on the FTIR spectra of orthoenstatite, especially at pressures of 1 to 2 GPa at which Al substitution in the tetrahedral site can be extensive (Mierdel et al. 2006). In aluminous enstatite, H_2O solubilities can approach 9000 ppmw at 900 °C and 1.5 GPa. In these enstatites, the O-H polarizations are strongest perpendicular to *c* (Mierdel et al. 2006).

Orthoenstatite is orthorhombic, *Pbca,* with two distinct tetrahedral sites, *T*1 and *T*2, arranged is separate layers of tetrahedral chains (Fig. 25). Al enters the structure as a coupled substitution where the Al is in both an *M*1 octahedron and one of the tetrahedral sites. Tetrahedral Al is known to strongly order in the structure with a very strong preference for *T*2 (Takeda 1973). There are six distinct oxygen sites in the structure, O1a, O1b, O2a, O2b, O3a,

and O3b, with the 'a' oxygens in the *T*1 chains and the 'b' oxygens in the *T*2 chains. The O3 atoms are the bridging oxygens in the chains. Electrostatic site potentials for the oxygens for pure Mg orthoenstatite are given in Table 3, and the O2b has the shallowest potential and is therefore the most likely site for protonation.

Structure refinement of a hydrous, aluminous orthopyroxene shows up to 5% cation vacancy at *M*2 with nearly equal amounts of Al substitution in both *M*1 and *T*2 sites, based on chemical analysis and volumes of coordination polyhedra (Smyth et al. 2006b). Also reported in Table 3 is an oxygen site potential calculation for a hypothetical fully "Mg-Tschermaks" orthoenstatite of composition $MgAlAlSiO_6$, fully ordered with all tetrahedral Al in *T*2. In this structure both O2b and O1b are substantially underbonded and likely sites for protonation. The O3b oxygen is also underbonded, but Al-avoidance would not allow Al in *T*2 to exceed 50%, so O3b is not as likely to protonate as O2b or O1b. It appears then that the major hydrous components are $MgAlAlSiO_6$ and $H_2AlAlSiO_6$ ("hydro-Tschermaks"), with a cation vacancy at *M*2 and protons on the O1b-O2b edges of the vacant *M*2 polyhedron, consistent with the observed O-H polarization in the *a*-*b* plane. This substitution mechanism achieves a net volume reduction of the unit cell, and nearly 1% H_2O by weight (Mierdel et al. 2006), but because it requires tetrahedral Al, H solubility decreases sharply with increasing pressure. The O2b and O1b oxygen sites are indicated by spheres in Figure 25.

This "hydro-Tschermaks" substitution appears to be strongly abetted by the ordering of tetrahedral Al in *T*2 which can only happen in the *Pbca* structure. At pressures near the 410 km discontinuity, enstatite is monoclinic, $P2_1/c$, after quenching to low temperature, but *C*2/*c* at relevant mantle temperatures. The solubility of H is much less than that in aluminous orthopyroxene at lower crustal pressure, so that clinoenstatite in equilibrium with forsterite containing >8000 ppmw H_2O contains less than 1000 ppmw (Smyth et al. 2006a) and somewhat less (~650 ppmw) in equilibrium with wadsleyite (Bolfan-Casanova et al. 2000). The principal substitution mechanism appears to be divalent cation vacancies, principally at *M*2.

Natural omphacites can contain up to about 3000 ppmw H_2O (Katayama and Nakashima 2003; Smyth et al. 1991). Bromiley and Keppler (2004) experimentally investigated water solubility in jadeite and found a maximum H_2O content of about 450 ppmw at 2 GPa, but dramatically higher solubilities in more complex solid solutions. Natural omphacites are very complex chemically containing 10% or more of up to eight chemical end members (Smyth 1980), but crystallographically relatively simple, having space group *C*2/*c* at mantle conditions of temperature and pressure. The hydrous component referred to as Ca-Eskola pyroxene $Ca_{0.5}\square_{0.5}AlSi_2O_6$, may be better described as $HAlSi_2O_6$. Crystal structure refinements of natural H-rich omphacites indicate significant *M*2 site vacancy (Smyth 1980). Textural evidence of kyanite and garnet exsolution from omphacite suggests that H_2O solubility in these pyroxenes may approach 1% by weight (Smyth et al. 1991). Bromiley et al. (2004) have experimentally hydrated natural Cr-diopside crystals at 1100 °C and pressures of 1.5 to 4 GPa. They report up to about 450 ppmw at 1.5GPa and infer proton positions on the O2-O1 and O2-O3 edges of the *M*2 polyhedron based on polarizations of the O-H vector in the *a*-*b* plane, which are similar to those reported for orthopyroxene by Mierdel et al. (2006).

Akimotoite

Akimotoite ($MgSiO_3$) is the ilmenite-type polymorph of enstatite stable at pressures of the lower transition zone (18-22 GPa). The structure is trigonal $R\bar{3}$ and has alternating layers of Si and Mg octahedra (Fig. 26). Bolfan-Casanova et al. (2000) report up to about 450 ppmw H_2O in pure Mg akimotoite at 21 GPa and 1500 °C coexisting with stishovite and melt. Bolfan-Casanova et al. (2000, 2002) report strongly pleochroic FTIR spectra for the O-H stretching vibration in this phase with strong absorptions at 3390 cm^{-1} parallel to *c* and 3320 and 3300 cm^{-1} perpendicular to *c*. Based on the polarizations and the relation of frequency to O-H-O

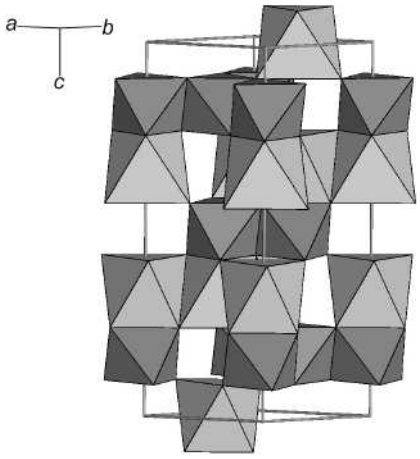

Figure 26. The structure of akimotoite (ilmenite-type $MgSiO_3$) is trigonal $R\bar{3}$ and closely related to that of corundum.

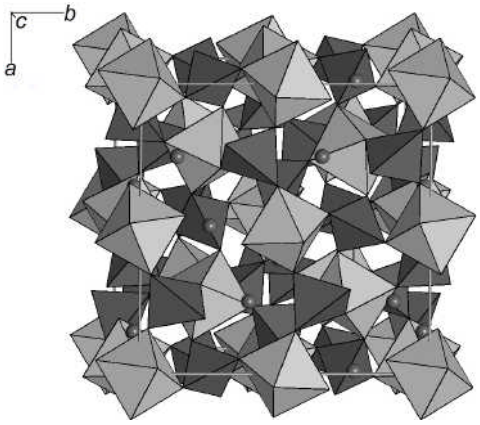

Figure 27. the structure of garnet is cubic $Ia\bar{3}d$. All oxygen atoms are identical and the tetrahedra and octahedra form a corner-sharing framework structure.

distance (Libowitzky 1999), they deduce two proton positions, both likely associated with Mg vacancies. Inasmuch as the structure is essentially isostructural with corundum, possible Al substitution for octahedral Si might have a significant impact on the H solubility in this phase.

Garnet

Garnet ($X_3Y_2Z_3O_{12}$) (Fig. 27) is isometric, $Ia\bar{3}d$, with Si (Z) in tetrahedral coordination forming a framework by sharing oxygens with Al (Y) in octahedral coordination. Interstitial to the framework is the dodecahedral divalent cation site, which may be occupied by Mg, Fe, or Ca (X). In this high-symmetry structure, all oxygens are equivalent and in a general position. At pressures of the transition zone, garnet can accept equal amounts of Si and Mg into the octahedral site in place of a trivalent cation. The $Mg_3(MgSi)_2Si_3O_{12}$ ($MgSiO_3$) end-member is majorite. Majorite quenches to tetragonal, $I4_1/a$, by ordering of Mg and Si in the octahedral site, although it is likely disordered $Ia\bar{3}d$ at mantle conditions (Angel et al. 1989). Hydrogen is accommodated in the garnet structure by Si vacancies so that the terminating octahedral oxygens are protonated. The tetrahedral site has $\bar{4}$ point symmetry, so symmetry constrains the oxygens to maintain a tetrahedral configuration, but the distance from the $\bar{4}$ point position to the oxygen increases from about 1.63 Å for the occupied site to about 1.95 Å for the vacant site (Lager and von Dreele 1996). This means that pressure inhibits the substitution so that garnets from high pressure environments generally contain less than 50 ppmw H_2O (Bell and Rossman 1992). Lager et al. (1987) and Lager and von Dreele (1996) report deuteron positions for a deuterated hydrogarnet ($Ca_3Al_2D_{12}O_{12}$) on the edges of the vacant tetrahedra based on neutron single crystal diffraction.

Olivine

Olivine ($(Mg,Fe)_2SiO_4$) is generally believed to be the most abundant phase in the upper mantle from the Moho to 410 km discontinuity. Natural olivines as reviewed in the current volume (Beran and Libowitzky 2006) contain up to about 400 ppm by weight (ppmw) H_2O, but typically less than 100 ppmw (Bell et al. 2004). Olivine synthesized at high pressures and quenched can contain much more H. Kohlstedt et al. (1996) report up to 1510 ppmw in olivine equilibrated at 1100 °C and 12 GPa. Recalculating this amount based on Bell et al. (2003) one

gets about 4000 ppmw (Hirschmann et al. 2005). Mosenfelder et al. (2006) report up to 6400 ppm H_2O in olivine quenched from 12 GPa and 1100 °C. Smyth et al. (2006a) report up to 8900 ppmw in olivine synthesized at 1250 °C and 12 GPa in equilibrium with either enstatite or clinohumite, but decreasing at higher temperatures with the onset of melting. Water contents approaching one per cent by weight would make olivine a major host for water in the upper mantle.

The olivine structure (Fig. 28) is orthorhombic, *Pbnm*, with two distinct octahedra, *M*1 and *M*2, and one silicate tetrahedron. There are three distinct oxygen sites in the structure, with O1 and O2 lying on the mirror, and O3 being in a general position. All oxygens are bonded to three Mg and one Si atom (Table 3) and site potentials range from 26.3 V for O3 to 27.7 V for O1. Smyth et al. (2006a) report that the major H substitution mechanism in olivine is protonation of the O1-O2 edges of vacant *M*1 octahedra. The proton position suggested by Smyth et al. (2006a) at $x/a = 0.95$; $y/b = 0.04$; $z/c = 0.25$ is illustrated in Figure 28. They further report a volume of hydration at ambient conditions:

$$V = 290.107 + 5.5\times10^{-5} * c_{H_2O}\ \text{Å}^3$$

where V is cell volume in Å^3, and H_2O is the ppm by weight H_2O as determined from the calibration of Bell et al. (2003).

Wadsleyite

Wadsleyite is the first high pressure polymorph of Mg_2SiO_4, and the olivine-wadsleyite transition at about 13 GPa is thought be responsible for the 410 km discontinuity. The wadsleyite structure (Fig. 29) is usually orthorhombic, *Imma*, with three distinct divalent metal octahedra, *M*1, *M*2 and *M*3. The structure is similar to that of spinelloid III in the Ni-aluminosilicate system (Ma and Sahl 1975). Unlike olivine which is based on a hexagonal close-packed array of oxygens, wadsleyite and the other spinels and spinelloids are based on a cubic close-packed oxygen array. Unlike olivine and ringwoodite, wadsleyite is a sorosilicate

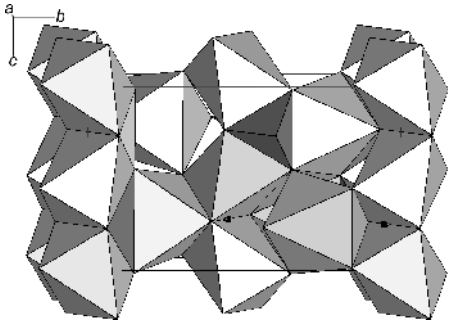

Figure 28. The structure of forsterite, Mg_2SiO_4, and fayalite Fe_2SiO_4, is orthorhombic *Pbnm*. Hydration appears to be compensated by octahedral cation vacancies principally at *M*1. The proton position inferred from polarized FTIR spectroscopy on the O1-O2 shared edge of the *M*1 octahedron is illustrated.

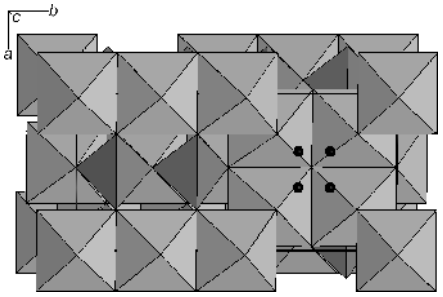

Figure 29. The structure of wadsleyite, $(Mg,Fe)_2SiO_4$, is orthorhombic *Imma.* Hydrous wadsleyite may deviate slightly from orthorhombic symmetry as monoclinic, *I*2/*m*, due to ordered cation vacancies in *M*3 in violation of the mirror perpendicular to *a*. The structure has a non-silicate oxygen which is readily protonated. Charge balance is maintained by Mg vacancies at *M*3.

with Si_2O_7 groups, a bridging oxygen (O2) and a non-silicate oxygen (O1). Smyth (1987) calculated oxygen site potentials and predicted that the under-bonded non-silicate oxygen would be a potential site for protonation. Wadsleyites with up to 3% by weight H_2O have been reported (Inoue et al. 1995). The major hydrogen substitution mechanism appears to be protonation of the vacant *M*3 octahedral edges and ordering of the vacancies so that hydrous wadsleyites with more than about 1% H_2O are monoclinic, *I*2/*m* (a subgroup of *Imma*). Beta angles up to 90.4° have been reported (Smyth et al. 1997; Jacobsen et al. 2005).

Wadsleyite shows a significant zero-pressure volume expansion that is similar in magnitude to that of olivine. Holl (2006) reports the volume expansion as:

$$V = 538.64 + 9.4 \times 10^{-5} * c_{H_2O} \text{ Å}^3$$

Hydrous wadsleyite shows a strong O-H stretching absorption at about 3325 cm^{-1} which shows minimal pleochroism. A potential proton location on the O1-O4 edge of a vacant M3 octahedron at about $x/a = 0.11$; $y/b = 0.20$; $z/c = 0.36$ would be consistent with the observed frequency and pleochroism of this polarization and is illustrated in Figure 29. The complexity of the infrared absorption spectrum, however, indicates that there are multiple possible proton locations in the structure (Kohn et al. 2002).

Wadsleyite II

Wadsleyite II is isostructural with spinelloid IV (Smyth and Kawamoto 1997; Smyth et al. 2005). It has only been reported from long-duration hydrous peridotite composition runs at 17.5 to 18 GPa, between the wadsleyite and ringwoodite fields. It is a well-ordered phase with *a*- and *c*-axes similar to wadsleyite but with a *b*-axis 2.5 times that of wadsleyite at about 30 Å. The structure is very difficult to distinguish from wadsleyite by powder diffraction or by Raman spectroscopy. The structure (Fig. 30) contains both isolated SiO_4 tetrahedra as well as Si_2O_7 groups in three distinct tetrahedral sites. It also contains six distinct octahedral sites and eight distinct oxygens, of which O2 is a non-silicate oxygen and a potential protonation site. Analogous to wadsleyite, a possible proton location would be near the O2-O4 edge of the *M*6 octahedron or the O2-O5 edge of the *M*5 octahedron. Wadsleyite II in the high pressure peridotite system is only known with about 2.8 wt% H_2O, whereas spinelloid IV in the Ni aluminosilicate system is thought to be anhydrous (Akaogi et al. 1982; Horioka et al. 1981).

Ringwoodite

Ringwoodite is the true spinel polymorph of forsterite and is stable as the dominant phase in a pyrolite composition mantle from about 525 to 670 km depth. The ringwoodite to perovskite plus periclase transition is thought to be responsible for the 670 km discontinuity. The structure (Fig. 31) is cubic, $Fd\bar{3}m$ with octahedral Mg and tetrahedral Si. Kohlstedt et al. (1996) report up to about 2.4 wt% H_2O in ringwoodite. The FTIR spectrum shows a

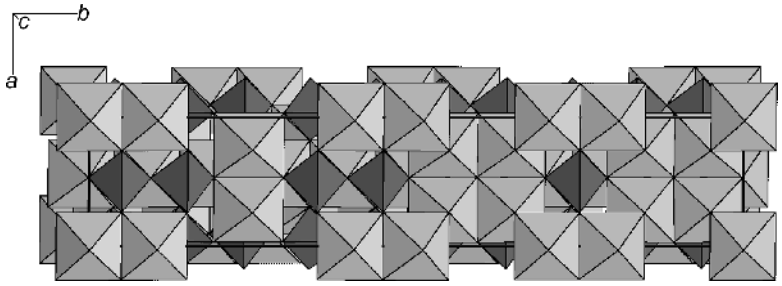

Figure 30. The structure of wadsleyite II, $(Mg,Fe)_2SiO_4$, is orthorhombic *Imma.* This structure, like wadsleyite is a spinelloid, but contains both isolated SiO_4 groups as well as Si_2O_7 groups.

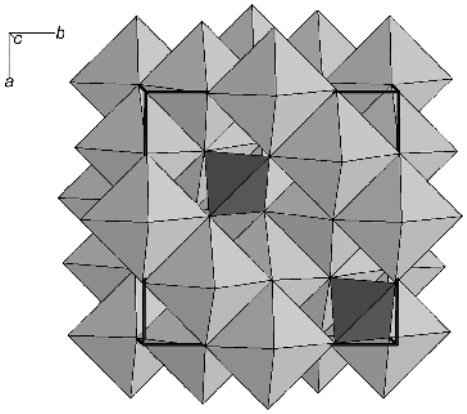

Figure 31. The structure of ringwoodite is a true spinel and is cubic, $Fd\bar{3}m$. Si is in tetrahedral (dark) and Mg in octahedral (light) coordination. All oxygens are equivalent and bonded to one Si and three Mg atoms. There are no bridging or non-silicate oxygens. Hydration is compensated by octahedral site vacancies.

broad absorption feature in the range 2600 to 3600 cm^{-1} (Smyth et al. 2003; Keppler and Smyth 2005). Although there is no IR pleochroism in the cubic system, the OH does appear to be structural because OH concentration computed from the FTIR spectrum correlates with a zero-pressure unit cell volume increase (Smyth et al. 2003) that is similar in magnitude to those observed for forsterite and wadsleyite cited above. Peaks in the spectra correlate with protonation of both the octahedral and tetrahedral edges (Libowitzky 1999) and crystal structure refinements indicate both octahedral and tetrahedral vacancies (Kudoh et al. 2000; Smyth et al. 2003).

Anhydrous phase B

Anhydrous phase B ($Mg_{14}Si_5O_{24}$) lies on the anhydrous edge of the DHMS ternary between forsterite and periclase. As with the other B-phases, anhydrous phase B has Mg/Si ratio greater than two, and so is not expected to coexist with either enstatite or majorite. It is therefore not expected to be a significant phase in the transition zone. The structure (Fig. 32) is orthorhombic, *Pmcb* (Hazen et al. 1992) and has Si in both octahedral and tetrahedral coordination. Little is known about its trace H content, but its oxygen sites are all electrostatically balanced according to Pauling bond strength sums, bonded to either three octahedral Mg and a tetrahedral Si, six Mg, or four Mg and one octahedral Si. Of these, the O4 is the non-silicate oxygen, has the lowest electrostatic potential and is thus a potential protonation site (Table 3). The density (3.39 g/cm^3) lies between that of forsterite and periclase, but less than either wadsleyite or ringwoodite, despite its octahedral silicon.

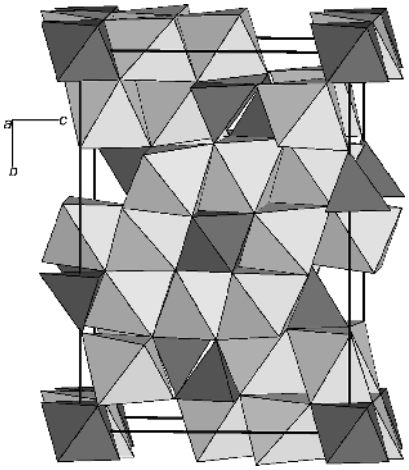

Figure 32. The structure of anhydrous Phase B (AnHB), $Mg_{14}Si_5O_{24}$, is orthorhombic *Pmcb*, and had Si in both octahedral and tetrahedral coordination.

Kyanite

Kyanite (Al_2SiO_5) is triclinic $P\bar{1}$, with Al in octahedral and Si in tetrahedral coordination. There are ten distinct oxygen sites in the structure (Fig. 33) most of which are bonded to two octahedral Al and one tetrahedral Si. The O2 and O6 positions are non-silicate oxygens and

bonded to only four Al atoms (Table 3). These are potential hydration sites if charge balance can be achieved by divalent cation substitution for Al. Although Beran and Goetzinger (1987) and Rossman and Smyth (1990) report relatively large amounts of OH in kyanite up to about 4000 ppmw H_2O, Bell et al. (2004) report a new calibration for kyanite, greatly reducing this amount and reporting a maximum H_2O content for kyanite of about 230 ppmw.

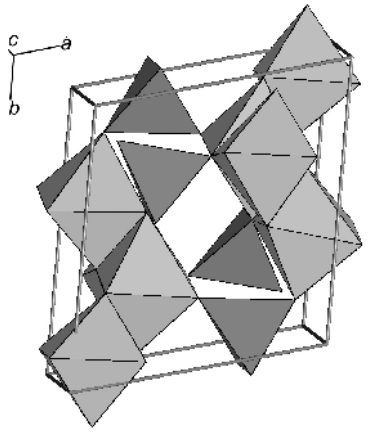

Figure 33. The structure of kyanite, Al_2SiO_5, is triclinic $P\bar{1}$.

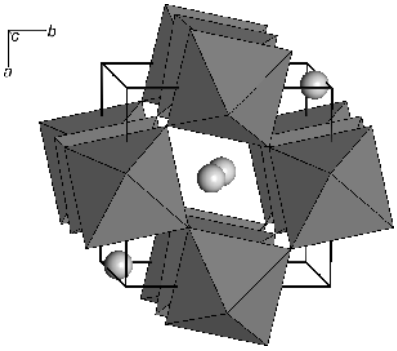

Figure 34. The structure of perovskite-type $MgSiO_3$ is orthorhombic *Pbnm*.

Perovskite

Perovskite-type $(Mg,Fe)SiO_3$ is believed to be the major phase in the lower mantle, so small amounts of H in this phase can have a large effect on the total water budget of the planet. The structure (Fig. 34) is orthorhombic, *Pbnm*, with Mg in eight coordination, Si in octahedral coordination, and two distinct oxygen sites. Both oxygen sites have relatively deep electrostatic potentials near 27 V (Table 3). The structure is dense (4.1 g/cm^3). Meade et al. (1994) report only minor amounts of H in $MgSiO_3$ perovskite. Bolfan-Casanova et al. (2000) report no detectable H by FTIR spectroscopy in pure $MgSiO_3$ perovskite in equilibrium with hydrous akimotoite in an Al-free composition, however Higo et al. (2001) report up to 500 ppmw H_2O by SIMS analysis of similar samples. Murakami et al. (2002) report up to 2000 ppmw H_2O in $(Mg,Fe)SiO_3$ perovskite synthesized at 25.5 GPa and 1600 °C in an Al-bearing peridotite composition. Litasov et al. (2003) observed only about 100 ppm in pure $MgSiO_3$ perovskite, but 1400 to 1800 ppmw H_2O in Al and Fe bearing perovskites in a hydrous peridotite system. None of the FTIR spectra of silicate perovskites in pure $MgSiO_3$ or $MgSiO_3$-Al_2O_3 systems show sharp absorption bands so there has been some disagreement as to whether these features represent structurally bound hydroxyl (Bolfan-Casanova et al. 2003; Litasov et al. 2003). Perovskite samples synthesized in chemically complex systems show a consistent but broad OH absorption feature at about 3397 cm^{-1}, but variable other features. It appears that while H_2O solubility in pure $MgSiO_3$ perovskite is likely negligible, perovskite crystallized from more chemically complex systems may incorporate significant amounts of water, but in reports of higher water contents, the possibility of hydrous inclusions within the perovskite cannot be ruled out.

Perovskite-type $CaSiO_3$ is believed to be a minor phase in the lower mantle. Although it is isostructural with $MgSiO_3$ perovskite (orthorhombic, *Pbnm*), is appears to form a separate phase in lower mantle synthesis experiments. Murakami et al. (2002) report up to 4000 ppmw H_2O in $CaSiO_3$ perovskite synthesized at 25.5 GPa and 1600 °C. This phase does not appear to be quenchable so interpretation of FTIR spectra on quenched material is difficult.

Post-perovskite

Post-perovskite ($MgSiO_3$) is a new structure type reported for $MgSiO_3$ at pressures of the lower-most lower mantle near the core-mantle boundary (Murakami et al. 2004). It is

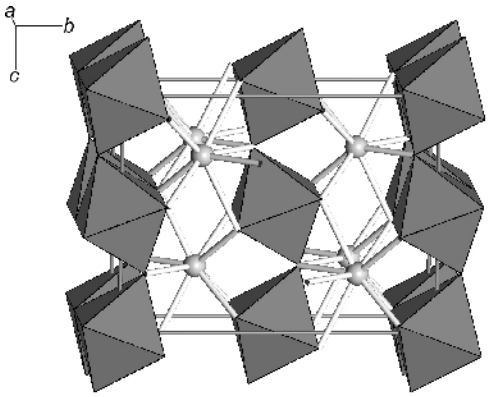

Figure 35. The structure of post-perovskite-type $MgSiO_3$ is orthorhombic *Cmcm*.

postulated that the perovskite to post perovskite transition may account for the discontinuity that defines the D″ layer near 2600 km depth. The structure (Fig. 35) is orthorhombic, *Cmcm*, and has edge-sharing silicate octahedra forming chains parallel to *a*, which are corner-linked to form sheets in the *a*-*c* plane. The sheets are linked together with 8-coodinated Mg atoms to form a strongly anisotropic structure. There are two distinct oxygen sites in the structure. Of these, O1 is slightly underbonded, being coordinated to two Si and two Mg atoms, whereas O2 is slightly overbonded to two Si and three Mg. However the potentials are rather similar to those of $MgSiO_3$-perovskite (Table 3).

Zircon

Zircon ($ZrSiO_4$) is a primary accessory phase in nearly all igneous rocks, and a major host phase for minor U, Th, and rare earth elements in the Earth. Though nominally anhydrous, non-metamict zircons of mantle origin can contain up to about 100 ppmw H_2O (Woodhead et al. 1991; Nasdala et al. 2001). This minor hydration is consistent with the very deep potential of the oxygen site (Table 3), and probably requires trivalent cation substitution for Zr. Additionally, metamict zircons, which have experienced radiation damage from the decay of U and Th, may contain much more H_2O, more than 16% by weight H_2O (Woodhead et al. 1991). The structure (Hazen and Finger 1979) is illustrated in Figure 36 and has Si in tetrahedral and Zr in eight-coordination. All O atoms are equivalent and bonded to tetrahedral Si so there are no non-silicate oxygens. Woodhead et al. (1991) report that strong absorption features at 3385 cm^{-1} perpendicular to *c,* and a weaker feature at 3420 cm^{-1} parallel to *c*, are associated with an occupied tetrahedron and trivalent cation substitution for Zr. However, if the proton is located on an O-O polyhedral edge, the only edge of the Zr polyhedron that does not have a component in the *c*-direction is the edge shared with the tetrahedron. This would be consistent with the suggestion of Nasdala et al. (2001) that hydration also appears to occur by the hydro-garnet substitution involving tetrahedral vacancy.

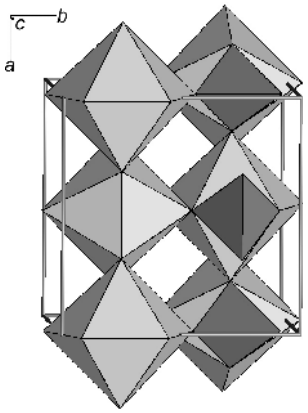

Figure 36. The structure of zircon, $ZrSiO_4$, is tetragonal, $I4_1/amd$. In this *c*-axis projection, the Zr is seen as eight-coordinated dipyramids (light) and the Si (dark) is tetrahedral. All oxygens are equivalent and bonded to two Zr and one Si.

Titanite

Titanite ($CaTiSiO_5$), like zircon, is a very common primary accessory phase in igneous rocks. The structure (Fig. 37) is monoclinic, $P2_1/a$ (*b*-unique) and has Ca in eight-coordination with Ti in octahedral and Si in tetrahedral coordination. Although it is nominally anhydrous, it can accommodate substantial amounts of both OH and F with Al substitution for Ti. There is one non-silicate oxygen in the structure (O1) which is bonded to one Ca and two Ti atoms. It is under-bonded in the Pauling sense, and its electrostatic site potential is 24.9 V which makes it the obvious candidate for protonation to accommodate Al or Fe^{3+} in the octahedron.

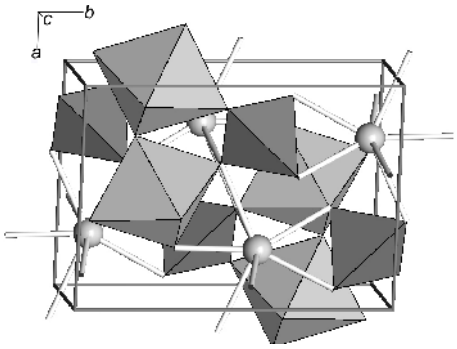

Figure 37. The structure of titanite, $CaTiSiO_5$, is monoclinic, $P2_1/a$.

CONCLUSIONS

The structure of the nominally hydrous and anhydrous phases that compose the Earth's mantle have been reviewed and compared. Among the nominally hydrous high-pressure silicate phases, we have examples of molecular water in lawsonite and K-cymrite. We also see that for hydroxyl-bearing silicates, the hydroxyls are in general, non-silicate oxygens. We see no examples of a proton on tetrahedral silicate oxygens. There are a few examples of protonated tetrahedral silicate oxygens in nature such as in the pyroxenoids, pectolite ($NaHCa_2Si_3O_9$) and serandite ($NaHMn_2Si_3O_9$). In these structures the chains are so strongly kinked that two of the non-bridging oxygens approach so closely that there is a H-bond between the two (Jacobsen et al. 2000). We also see a few examples of Si-OH bonds for octahedral silica, as in the very high pressure phases D and Egg. This is consistent with the octahedral Si-O bond being longer and weaker than the tetrahedral Si-O bond. Among the nominally anhydrous phases we see that the phases that have only bridging tetrahedral silicate oxygens are able to accommodate the least amount of H, whereas phases containing non-silicate oxygens are readily hydrated. The minerals containing octahedral silica can accept up to several thousand ppmw H_2O if Al is present to substitute for octahedral silica.

ACKNOWLEDGMENT

The author thanks U.S. National Science Foundation for grant NSF-EAR 03-36611, the Bayerisches Geoinstitut Visitors Program, and the Alexander von Humboldt Foundation. The author also thanks H. Keppler, T. Boffa-Balaran and P. Comodi for constructive, thorough, and competent reviews.

REFERENCES

Akaogi M, Akimoto S, Horioka H, Takahashi K, Horiuchi H (1982) The system $NiAl_2O_4$-Ni_2SiO_4 at high pressures ad high temperatures: spinelloids with spinel-related structures. J Solid State Chem 44:257-267

Angel RJ, Finger LW, Hazen RM, Kanzaki M, Weidner DJ, Liebermann RC, Veblen DR (1989) Structure and twinning of single-crystal $MgSiO_3$ garnet synthesized at 17 GPa and 1800 C. Am Mineral 74:509-512

Armbruster T, Geiger CA, Lager G (1992) Single crystal X-ray study of synthetic pyrope almandine garnets at 100 and 293 K. Am Mineral 77:512-521

Baur WH (1978) Crystal structure refinement of lawsonite. Am Mineral 63:311-315
Beard JS (2000) Occurrence and composition of tochilinite and related minerals in Site 1068 serpentinites. *In:* Proceedings of the Ocean Drilling Program, Scientific Results, Return to Iberia. Beslier M-O, Whitmarsh RB, Wallace PJ, Girardeau J (eds) OPD, 173:1–9
Bell DR, Rossman GR (1992) Water in the Earth's mantle: Role of nominally anhydrous minerals. Science 255: 1392-1396
Bell DR, Rossman GR, Moore RO (2004) Abundance and partitioning of OH in a high-pressure magmatic system: megacrysts from the Monastery Kimberlite, South Africa. J Petrol 45:1539-1564
Bell DR, Rossman GR, Maldener J, Endisch D, Rauch F (2004) Hydroxide in kyanite: A quantitative determination of the absolute amount and calibration for the IR spectrum. Am Mineral 89:998-1003
Bell DR, Rossman GR, Maldener J, Endisch D, Rauch F (2003) Hydroxide in olivine: a quantitative determination of the absolute amount and calibration of the IR spectrum. J Geophys Res 108 doi:10.1029/2001JB000679
Beran A, Goetzinger MA (1987) Quantitative IR spectroscopic determination of structural OH groups in kyanites. Mineral Petrol 36:41-49
Bercovici D, Karato S-I (2003) Whole-mantle convection and the transition-zone water filter. Nature 425:39-44
Beran A, Libowitzky E (2006) Water in natural mantle minerals II: olivine, garnet and accessory minerals. Rev Mineral Geochem 62:169-191
Berry A, James M (2001) Refinement of hydrogen positions in synthetic hydroxyl clinohumite by powder neutron diffraction. Am Mineral 86:181-184
Boffa-Balaran T, Angel RJ (2003) Equation of state and high-pressure phase transitions in lawsonite. Eur J Min 15:241-246
Bolfan-Casanova N, Keppler H, Rubie DC (2002) Hydroxyl in $MgSiO_3$ akimotoite: a polarized and high pressure IR study. Am Mineral 87:603-608
Bolfan-Casanova N, Mackwell S, Keppler H, McCammon CA, Rubie DC (2002) Pressure dependence of H solubility in magnesiowustite up to 25 GPa: Implications for the storage of water in the Earth's lower mantle. Geophys Res Lett 29:1029-1032
Bolfan-Casanova N, Keppler H, Rubie DC (2003) Water partitioning at the 660 km discontinuity and evidence for very low water solubility in magnesium silicate perovskite. Geophys Res Lett 30:1905-1908
Bolfan-Casanova N, Keppler H, Rubie DC (2000) Water partitioning between nominally anhydrous minerals in the MgO-SiO_2-H_2O system up to 24 GPa: implications for the distribution of water in the Earth's mantle. Earth Planet Sci Lett 182:209-221
Bromiley GD, Keppler H (2004) An experimental investigation of hydroxyl solubility in jadeite and Na-rich clinopyroxenes. Contrib Mineral Petrol 147:189–200
Bromiley GD, Keppler H, McCammon C, Bromiley FA, Jacobsen SD (2004) Hydrogen solubility and speciation in natural, gem-quality chromian diopside. Am Mineral 89:941–949
Burnley PC, Navrotsky A (1996) Synthesis of high-pressure hydrous magnesium silicates: observations and analysis. Am Mineral 81:317–326
Cameron M, Sueno S, Prewitt CT, Papike JJ (1973) High temperature crystal chemistry of acmite, diopside, hedenbergite, jadeite, spodumene, and ureyite. Am Mineral 58:594-618
Coes L (1962) Synthesis of minerals at high pressures. *In:* Modern Very High Pressure Techniques. Wentorf R (ed) Butterworths, p 137-150
Comodi P, Fumagalli P, Nazzareni S, Zanazzi PF (2005) The 10 Å phase: Crystal structure from single-crystal X-ray data. Am Mineral 90:1012-1016
Daniels P, Wunder B (1993) Crystal structure of tri-aluminium tri-hydroxo disilicate, $Al_3Si_2O_7(OH)_3$. Z Kristallogr 206:103-105
Daniels P, Wunder B (1996) Crystal structure of phase Pi, $Al_3Si_2O_7(OH)_3$. Eur J Min 8 1283
Domanik K, Holloway JR (1996): The stability and composition of phengitic muscovite and associated phases from 5.5 to 11 GPa: Implications for deeply subducted sediments. *Geochim. Cosmochim Acta* **64:**4133-4150
Eggleton RA, Boland JN, Ringwood AE (1978) High-pressure synthesis of a new aluminum silicate: $Al_5Si_5O_{17}OH$. Geochem J 12:191–194
Fasshauer DW, Chatterjee ND, Marler B (1997) Synthesis, structure, thermodynamic properties and stability relations of K-cymrite. Phys Chem Minerals 24:455-462
Finger LW, Hazen RM, Zhang J, Ko J, Navrotsky A (1993) The effect of Fe on the crystal structure of wadsleyite β-$(Mg1\text{-}xFex)_2SiO4$, $0.00 < x < 0.40$. Phys Chem Minerals 19:361-368
Finger LW, Ko J, Hazen RM, Gasparik T, Hemley RJ, Prewitt CT, Weidner DJ (1989) Crystal chemistry of Phase B and an anhydrous analogue: Implication for water storage in the mantle. Nature 341:140-142
Franz G, Liebscher A (2004) Physical and chemical properties of the epidote minerals – an introduction. Rev Mineral Geochem 56:1-81

Friedrich A, Lager GA, Kunz M, Chakoumakos BC, Smyth JR, Schultz AJ (2001) Temperature-dependent single-crystal neutron diffraction study of natural chondrodite and clinohumite. Am Mineral 86:981-989
Frost DJ, Fei Y (1999) Static compression of the hydrous magnesium silicate phase D to 30 GPa at room temperature. Phys Chem Minerals 26:415-418
Fujino K, Sasaki S, Takeuchi Y, Sadanaga R (1981) X-ray determinations of electron distributions in forsterite, fayalite, and tephroite. Acta Crystallogr B 37:513-518
Fumagalli P, Poli S (2005) Experimentally determined phase relations in hydrous peridotites to 6.5 GPa and their consequences on the dynamics of subduction zones. J Petrol 46:555–578
Fumagalli P, Stixrude L, Poli S, Snyder D (2001) The 10 Å phase: a high-pressure expandable sheet silicate stable during subduction of hydrated lithosphere. Earth Planet Sci Lett 186:125-141
Gabe EJ, Portheine JC, Whitlow SH (1973) A reinvestigation of the epidote structure: confirmation of the iron location. Am Mineral 58:212-253
Grevel K-D, Nowlan, EU, Fasshauer DW, Burchard M (2000) X-ray diffraction analysis of lawsonite and zoisite at high pressures and temperatures. Am Mineral 85:206-216
Hawthorne FC, Grundy HD (1976) The crystal chemistry of the amphiboles IV. X-ray and neutron refinements of the crystal structure of tremolite. Can Mineral 14:334-345
Hazen RM (1976) Effects of temperature and pressure on the cell dimension and X-ray temperature factors of periclase. Am Mineral 61:266-271
Hazen RM (1981) Systematic variation of bulk modulus of wüstite with stoichiometry. Carnegie Inst Wash Yearb 80:277-280
Hazen RM, Burnham CW (1973) The crystal structures of one-layer muscovite and annite. Am Mineral 58: 889-900
Hazen RM, Finger LW (1979) Crystal structure and compressibility of zircon at high pressure. Am Mineral 64: 196-201
Hazen RM, Finger LW, Ko J (1992) Crystal chemistry of Fe-bearing anhydrous phase B: Implications for transition zone mineralogy. Am Mineral 77:217-220
Higo Y, Inoue T, Irifune T, Yurimoto H (2001) Effect of water on the spinel-postspinel transformation in Mg_2SiO_4. Geophys Res Lett 28:3505-3508
Hirschmann MM, Aubaud C, Withers AC (2005) Storage capacity of H_2O in nominally anhydrous minerals in the upper mantle. Earth Planet Sci Lett 236:167-181
Holl CM (2006) Effects of hydration on the structure and compression of wadsleyite: Implications for water in the Earth's interior. Ph.D. Dissertation Geological Sciences, University of Colorado, Boulder.
Horioka K, Takahashi K, Morimoto N, Horiuchi H, Akaogi M, Akimoto S (1981) Structure of nickel aluminosilicate (Phase IV): A high-pressure phase related to spinel. Acta Crystallogr B37:635-638
Horiuchi H, Morimoto N, Yamamoto K, Akimoto S (1979) Crystal structure of $2Mg_2SiO_4 \cdot 3Mg(OH)_2$, a new high-pressure structure type. Am Mineral 64:593-598
Horiuchi H, Hirano M, Ito E, Matsui Y (1982) $MgSiO_3$ (ilmenite-type): Single crystal X-ray diffraction study. Am Mineral 67:788-793
Horiuchi H, Ito E, Weidner D (1987) Perovskite-type $MgSiO_3$: Single-crystal X-ray diffraction study. Am Mineral 72:357-360
Huang X, Xu Y, Karato SI (2005) Water content of the transition zone form electrical conductivity of wadsleyite and ringwoodite. Nature 434:746-749
Inoue T, Yurimoto H, Kudoh Y (1995) Hydrous modified spinel, $Mg_{1.75}SiH_{0.5}O_4$: a new water reservoir in the mantle transition region. Geophys Res Lett 22:117-120
Jacobsen SD (2006) Effect of water on the equation of state of nominally anhydrous minerals. Rev Mineral Geochem 62:321-342
Jacobsen SD, Smyth JR (2006) Effect of water on the sound velocities of ringwoodite in the transition zone. Earth's Deep Water Cycle, AGU Monograph Series (in press)
Jacobsen SD, Lin JF, Angel RJ, Shen G, Prakapenka VB, Dera P, Mao HK, and Hemley RJ (2005) Single-crystal synchrotron X-ray diffraction study of wüstite and magnesiowüstite at lower-mantle pressures. J Synchr Rad 12:577-583
Jacobsen SD, Demouchy S, Frost DJ, Boffa-Ballaran T, Kung J (2005) A systematic study of OH in hydrous wadsleyite from polarized FTIR spectroscopy and single-crystal X-ray diffraction: Oxygen sites for hydrogen storage in the Earth's interior. Am Mineral 90:61-70
Jacobsen SD, Smyth JR, Spetzler H, Holl CM, Frost DJ, (2004) Sound velocities and elastic constants of iron-bearing hydrous ringwoodite. Phys Earth Planet Int 143-144:47-56
Jacobsen SD, Smyth JR, Swope RJ, Sheldon RI (2000) Two proton positions in the very strong H-bond of serandite [$Na,Mn_2Si_3O_8OH$]. Am Mineral 85:745-752
Libowitzky E, Beran A (2006) The structure of hydrous species in nominally anhydrous minerals: information from polarized IR spectroscopy. Rev Mineral Geochem 62:29-52

Kagi H, Parise JB, Cho HM, Rossman GR, Loveday JS (2000) Hydrogen bonding interactions in phase A [$Mg_7Si_2O_8(OH)_6$] at ambient and high pressure. Phys Chem Minerals 27:225–233

Kanzaki M (1991) Stability of hydrous magnesium silicates in the mantle transition zone. Phys Earth Planet Int 66:307–312

Karato S (1990) The role of hydrogen in the electrical conductivity of the upper mantle. Nature 347:272-273

Karato S, Paterson MS, Fitzgerald D (1986) Rheology of synthetic olivine aggregates: Influence of grain size and water. J Geophys Res 91:8151-8176

Kavner A (2003) Elasticity and strength of hydrous ringwoodite at high pressure. Earth Planet Sci Lett 214: 645-654

Katayama I, Nakashima S (2003) Hydroxyl in clinopyroxene from the deep subducted crust: Evidence for H_2O transport into the mantle. Am Mineral 88:229-234

Kawamoto T, Hervig RL, Holloway JR (1996) Experimental evidence for a hydrous transition zone in the early Earth's mantle. Earth Planet Sci Lett 142:587-592

Kek S, Aroyo M, Bismayer U, Schmidt C, Eichhorn K, Krane HG (1997) The two-step phase transition of titanite, $CaTiSiO_5$: a synchrotron radiation study. Zeit Kristallogr 212:9–19

Keppler H, Smyth JR (2005) Optical and near infrared spectra of ringwoodite to 21.5 GPa. Am Mineral 90: 1209-1214

Kihara K (1990) An X-ray study of the temperature dependence of the quartz structure. Eur J Mineral 2:63-77

Koch-Mueller M, Dera P, Fei Y, Hellwig H, Liu Z, Van Orman J, Wirth R (2005) Polymorphic phase transition in superhydrous phase B. Phys Chem Minerals 32:349-361

Koch-Müller M, Dera P, Fei Y, Reno B, Sobolev N, Hauri E, Wysoczanski R (2003) OH- in synthetic and natural coesite. Am Mineral 88:1436-1445

Koch-Müller M, Fei Y, Hauri E, Liu Z (2001) Location and quantitative analysis of OH in coesite. Phys Chem Minerals 28:693-705

Kohlstedt DL, Keppler H, Rubie DC (1996) Solubility of water in the α, β, and γ phases of $(Mg,Fe)_2SiO_4$. Contr Mineral Petrol 123:345-357

Kohn SC, Brooker RA, Frost DJ, Slesinger AE, Wood BJ (2002) Ordering of hydroxyl defects in hydrous wadsleyite (β-Mg_2SiO_4). Am Mineral 87:293-301

Kudoh Y, Kuribayashi T, Mizohata H, Ohtani E (2000) Structure and cation disorder of hydrous ringwoodite, γ-$Mg_{1.89}Si_{0.97}H_{0.34}O_4$. Phys Chem Minerals 27:474-479

Kudoh Y, Finger LW, Hazen RM, Prewitt CT, Kanzaki M, Veblen DR (1993) Phase E: a high pressure hydrous silicate with unique crystal chemistry. Phys Chem Minerals 19:357-360

Lager GA, Von Dreele RB (1996) Neutron powder diffraction study of hydrogarnet to 9.0 GPa. Am Mineral 81: 1097-1104

Lager GA, Marshall WG, Liu Z, Downs RT (2005) Re-examination of the hydrogarnet structure at high pressure using neutron powder diffraction and infrared spectroscopy. Am Mineral 90:639-644

Lager GA, Ulmer P, Miletich R, Marshall WG (2001) O-D...O bond geometry in OD-chondrodite. Am Mineral 86:176-180

Lager GA, Armbruster T, Faber J (1987) Neutron and X-ray diffraction study of hydrogarnet $Ca_3A1_2(O_4H_4)_3$. Am Mineral 72:756–765

Libowitzky E (1999) Correlation of O-H stretching frequencies and O-H. . .O hydrogen bond lengths in minerals. Monatsh. Chemie 130:1047-1059

Litasov K, Ohtani E, Langenhorst F, Yurimoto H, Kubo T, Kondo T (2003) Water solubility in Mg-perovskites and wate storage capacity in the lower mantle. Earth Planet Sci Lett 211:189-203

Luth RW (1995) Is phase A relevant to the Earth's mantle? Geochim Cosmochim Acta 59:679-682

Ma C-B, Sahl K (1975) Nickel aluminosilcate, phase III. Acta Crystallogr B31:2142-2143

Meade C, Reffner JA, Ito E (1994) Synchrotron infrared absorbance measurements of hydrogen in $MgSiO_3$ perovskite. Science 264:1558–1560

Mellini M (1982) The crystal structure of lizardite 1T: Hydrogen bonds and polytypism. Am Mineral 67:587-598

Mierdel K, Keppler H (2004) The temperature dependence of water solubility in enstatite. Contrib Mineral Petrol 148:305–311

Mierdel K, Kepler H, Smyth JR, Langenhorst F (2006) The origin of the Earth's asthenosphere. Nature (in review)

Mosenfelder JL (2000) Pressure dependence of hydroxyl solubility in coesite. Phys Chem Minerals 27:610-617

Mosenfelder JL, Deligne NI, Asimow PD, Rossman GR (2006) Hydrogen incorporation into olivine at 2-12 GPa. Am Mineral 91:285-294

Murakami M, Hirose K, Yurimoto H, Nakashima S, Takafuji N (2002) Water in the Earth's lower mantle. Science 295:1885-1887

Murakami M, Hirose K, Kawamura K, Sata N, Ohishi Y (2004) Post-perovskite phase transition in $MgSiO_3$. Science 304:855-858

Nasdala L, Beran A, Libowitzky E, Wolf D (2001) The incorporation of hydroxyl groups and molecular water in natural zircon ($ZrSiO_4$). Am J Sci 301:831-857

Newnham RE, deHaan YM (1962) Refinement of the alpha-Al_2O_3, Ti_2O_3, V_2O_3, and Cr_2O_3 structures. Z Kristallogr 117:235-237

Northrup PA, Leinenweber K, Parise JB (1994) The location of H in the high-pressure synthetic $Al_2SiO_4(OH)_2$ topaz analogue. Am Mineral 79:401-404

Pacalo REG, Parise JB (1992) Crystal structure of superhydrous B, a hydrous magnesium silicate synthesized at 1400 °C and 20 GPa. Am Mineral 77:681-684

Pannhorst W (1984) High temperature crystal structure refinements of low clinoenstatite up to 700 °C. N Jahrb Mineral Abh 150:219-228

Pawley AR (1994) The pressure and temperature stability limits of lawsonite: implications for H_2O recycling in subduction zones. Contr Mineral Petrol 118:99-108

Pawley AR, Redfern SAT, Holland TJB (1996) Volume behavior of hydrous minerals at high pressure and temperature: 1. Thermal expansion of lawsonite, zoisite, clinozoisite, and diaspore. Am Mineral 81:335-340

Perdikatsis B, Burzlaff H (1981) Strukturverfeinerung am Talk $Mg_3[(OH)_2Si_4O_{10}]$. Z Kristalogr 156:177-186

Poli S, Schmidt MW (2004) Experimental subsolidus studies of epidote minerals. Rev Mineral Geochem 56: 171-195

Rauch M, Keppler H (2002) Water solubility in orthopyroxene. Contrib Mineral Petrol 143:525-536

Ross NL, Crichton WA (2001) Compression of synthetic hydroxyl clinohumite [Mg9Si4O16(OH)2] and hydroxyl chondrodite [Mg5Si2O8(OH)2]. Am Mineral 86:990-996

Ross NL, Gibbs GV, Rosso KM (2003) Potential docking sites and positions of hydrogen in high-pressure silicates. Am Mineral 88:1452-1459

Ross NL, Shu JF, Hazen RM, Gasparik T (1990) High-pressure crystal chemistry of stishovite. Am Mineral 75: 739-747

Rossman GR, Smyth JR (1990) Hydroxyl contents of accessory minerals in mantle eclogites and related rocks. Am Mineral 75:775-780

Rothbauer R. (1971) Untersuchung eines $2M_1$-Muskovits mit Neutronenstrahlung. Neues J Mineral Monats 1971:143-154

Schilling FR, Sinogeikin SV, Bass JD (2003) Single-crystal elastic properties of lawsonite and their variation with temperature. Phys Earth Planet Inter 136:107-118

Schmidt MW, Poli S (1998) Experimentally based water budgets for dehydrating slabs and consequences for arc magma generation. Earth Planet Sci Lett 163:361-179

Schmidt MW, Finger LW, Angel RJ, Dinnebier RE (1998) Synthesis, crystal structure and phase relations of $AlSiO_3OH$, a high pressure hydrous phase. Am Mineral 83:881-888

Shieh SR, Mao HK, Konzett J, Hemley RJ (2000) In-situ high pressure X-ray diffraction of phase E to 15 GPa. Am Mineral 85:765-769

Shintani H, Sato S, Saito Y (1975) Electron density distribution in rutile crystals. Acta Crystallogr B31:1981-1982

Shu J, Mao HK, Hu J, Fei Y, Hemley RJ (1998) Single-crystal X-ray diffraction of wüstite to 30 GPa hydrostatic pressure. N Jahrb Mineral Abh 172:309–323

Skogby H (2006) Water in natural mantle minerals I: pyroxenes. Rev Mineral Geochem 62:155-167

Smyth JR (1980) Cation vacancies and the crystal chemistry of breakdown reactions in kimberlitic omphacites. Am Mineral 65:1185-1191

Smyth JR (1987) β-Mg_2SiO_4: a potential host for water in the mantle? Am Mineral 72:1051-1055

Smyth JR (1989) Electrostatic characterization of oxygen sites in minerals. Geochim Cosmochim Acta 53: 1101-1110

Smyth JR, Artioli G, Smith JV, Kvick A (1987) Crystal structure of coesite a high pressure form of SiO_2 at 15 and 298 K from single crystal neutron and X-ray diffraction data: test of bonding models. J Phys Chem 91:988-992

Smyth JR, Dyar MD, May HH, Bricker OP, and Acker HA (1997) Crystal structure refinement and Mössbauer spectroscopy of an ordered triclinic chlorite. Clays Clay Mineral 45:544-550

Smyth JR, Frost DJ (2002) The effect of water on the 410-km discontinuity: an experimental study. Geophys Res Lett 29:1485, doi:10.1029/2001GL014418

Smyth JR, Kawamoto T (1997) Wadsleyite II: A new high pressure hydrous phase in the peridotite-H_2O system. Earth Planet Sci Lett 146:E9-E16

Smyth JR, Frost DJ, Nestola F, Holl CM, Bromiley G (2006a) Olivine hydration in the deep upper mantle: effects of temperature and silica activity. Geophys Res Lett 33, doi:2006GL026194 (in press)

Smyth JR, Holl CM, Frost DJ, Jacobsen SD, (2004) High pressure crystal chemistry of hydrous ringwoodite and water in the Earth's interior. Phys Earth Planet Int 143-144:271-278

Smyth JR, Holl CM, Frost DJ, Jacobsen SD, Langenhorst F, McCammon CA (2003) Structural systematics of hydrous ringwoodite and water in the Earth's interior. Am Mineral 88:1402-1407

Smyth JR, Holl CM, Langenhorst F, Laustsen HMS, Rossman GR, Kleppe A, McCammon CA, Kawamoto T, van Aken PA (2005) Crystal chemistry of wadsleyite II and water in the Earth's interior. Phys Chem Minerals 31:691-705

Smyth JR, Jacobsen SD, Swope RJ, Angel RJ, Arlt T, Domanik K, Holloway JR (2000) Crystal structures and compressibilities of synthetic $2M_1$ and 3T phengite micas. Eur J Mineral 12:955-963

Smyth JR, Kawamoto T, Jacobsen SD, Swope RJ, Hervig RL, Holloway JR (1997) Crystal structure of monoclinic hydrous wadsleyite. Am Mineral 82:270-275

Smyth JR, Mierdel K, Keppler H, Langenhorst F, Dubrovinsky L, Nestola F (2006b) Crystal chemistry of hydration in aluminous orthopyroxene. American Mineralogist (in prep.)

Smyth JR, Rossman GR, Bell DR (1991) Incorporation of hydroxyl in upper mantle clino-pyroxenes. Nature 351:732-735

Smyth JR, Swope RJ, Pawley AJ (1995) H in rutile-type compounds: II. Crystal chemistry of Al substitution in H-bearing stishovite. Am Mineral 80:454-456

Sueno S, Cameron M, Prewitt CT (1976) Orthoferrosilite: High temperature crystal chemistry. Am Mineral 61: 38-53

Swope RJ, Smyth JR, Larson AC (1995) H in rutile-type compounds: I. Single-crystal neutron and X-ray diffraction study of H in rutile. Am Mineral 80:448-453

Takeda H (1973) Tetrahedral sizes of orthopyroxenes and silicon-aluminum ordering. Am Mineral 58:1096-1097

Vlassopoulos D, Rossman GR, Haggerty SE (1993) Coupled substitution of H and minor elements in rutile and the implications of high OH contents in Nb- and Cr-rich rutile from the upper mantle. Am Mineral 78: 1181-1191

Vanpeteghem CB, Ohtani E, Kondo T, Takemura K, Kikegawa T (2003) Compressibility of phase Egg $AlSiO_3OH$: Equation of state and role of water at high pressure. Am Mineral 88:1408-1411

Winter JK, Ghose S (1979) Thermal expansion and high temperature crystal chemistry of the Al_2SiO_5 polymorphs. Am Mineral 64:573-586

Wood BJ (1995) The effect of H_2O on the 410-kilometer seismic discontinuity. Science 268:74-76

Woodhead JA, Rossman GR, Thomas AP (1991) Hydrous species in zircon. Am Mineral 76:1533-1546

Wunder B (1998) Equilibrium experiments in the system MgO-SiO_2-H_2O (MSH): stability fields of clinohumite-OH [$Mg_9Si_4O_{16}(OH)_2$], chondrodite-OH [$Mg_5Si_2O_8(OH)_2$] and phase A [$Mg_7Si_2O_{16}(OH)_6$]. Contr Mineral Petrol 132:111-120

Wunder B, Andrut M, Wirth R (1999) High pressure synthesis and properties of OH-rich topaz. Eur J Mineral 11:803-813

Wunder B, Medenbach O, Daniels P, Schreyer W (1995) First synthesis of the hydroxyl end-member of humite $Mg_7Si_3O_{12}(OH)_2$. Am Mineral 80:638-640

Wunder B, Medenbach O, Krause W, Schreyer W (1993)Synthesis, properties and stability of $Al_3Si_2O_7(OH)_3$ (phase Pi), a hydrous high-pressure phase in the system Al_2O_3-SiO_2-H_2O (ASH). Eur J Mineral 5:637-649

Yamamoto K, Akimoto S (1977) The system MgO-SiO_2-H_2O at high pressure and temperatures – stability field for hydroxyl-chondrodite, hydroxyl-clinohumite, and 10 Å-phase. Am J Sci 277:288-312

Yagi T, Marumo F, Akimoto S (1974) Crystal structures of spinel polymorphs of Fe_2SiO_4 and Ni_2SiO_4. Am Mineral 59:486-490

Yang H, Prewitt CT (2000) Chain and layer silicates at high temperatures and pressures. Rev Mineral Geochem 41:211-256

Yang H, Prewitt CT, Frost DJ (1997) Crystal structure of the dense hydrous magnesium silicate, phase D. Am Mineral 82:651-654

Yang H, Hazen RM, Prewitt CT, Finger LW, Lu R, Hemley RJ (1998) High-pressure single-crystal X-ray diffraction and infrared spectroscopic studies of *C*2/*m*-*P*2_1/*m* phase transition in cummingtonite. Am Mineral 83:288-299

Yang H, Ghose S (1995) High temperature single crystal X-ray diffraction study of the ortho-proto phase transition in enstatite $Mg_2Si_2O_6$. Phys Chem Minerals 22:300-310

Zigan F, Rothbauer R (1967) Neutronenbeugungsmessung am Brucit. N Jahrb Mineral Monats 137-143